Toxicology and Applied Pharmacology 283 (2015) 210–222

Contents lists available at ScienceDirect

Toxicology and Applied Pharmacology

journal homepage: www.elsevier.com/locate/ytaap

Changes in cholesterol homeostasis and acute phase response link pulmonary exposure to multi-walled carbon nanotubes to risk of cardiovascular disease

Sarah S. Poulsen [a,b,*], Anne T. Saber [a], Alicja Mortensen [c], Józef Szarek [d], Dongmei Wu [e], Andrew Williams [e], Ole Andersen [b], Nicklas R. Jacobsen [a], Carole L. Yauk [e], Håkan Wallin [a,f], Sabina Halappanavar [e], Ulla Vogel [a,g]

[a] National Research Centre for the Working Environment, DK-2100 Copenhagen, Denmark
[b] Department of Science, Systems and Models, Roskilde University, DK-4000 Roskilde, Denmark
[c] National Food Institute, Technical University of Denmark, Søborg, Denmark
[d] Faculty of Veterinary Medicine, University of Warmia and Mazury in Olsztyn, 10-719 Olsztyn, Poland
[e] Environmental and Radiation Health Sciences Directorate, Health Canada, Ottawa, Ontario K1A 0K9, Canada
[f] Department of Public Health, University of Copenhagen, DK-1014 Copenhagen K, Denmark
[g] Department of Micro- and Nanotechnology, Technical University of Denmark, DK-2800 Kgs. Lyngby, Denmark

ARTICLE INFO

Article history:
Received 24 October 2014
Revised 7 January 2015
Accepted 12 January 2015
Available online 22 January 2015

Keywords:
Nanotoxicology
Atherosclerosis
Toxicogenomics
Liver
Acute phase response
Histology

ABSTRACT

Adverse lung effects following pulmonary exposure to multi-walled carbon nanotubes (MWCNTs) are well documented in rodents. However, systemic effects are less understood. Epidemiological studies have shown increased cardiovascular disease risk after pulmonary exposure to airborne particles, which has led to concerns that inhalation exposure to MWCNTs might pose similar risks.

We analyzed parameters related to cardiovascular disease, including plasma acute phase response (APR) proteins and plasma lipids, in female C57BL/6 mice exposed to a single intratracheal instillation of 0, 18, 54 or 162 μg/mouse of small, entangled (CNT_{Small}, 0.8 ± 0.1 μm long) or large, thick MWCNTs (CNT_{Large}, 4 ± 0.4 μm long). Liver tissues and plasma were harvested 1, 3 and 28 days post-exposure. In addition, global hepatic gene expression, hepatic cholesterol content and liver histology were used to assess hepatic effects.

The two MWCNTs induced similar systemic responses despite their different physicochemical properties. APR proteins SAA3 and haptoglobin, plasma total cholesterol and low-density/very low-density lipoprotein were significantly increased following exposure to either MWCNTs. Plasma SAA3 levels correlated strongly with pulmonary *Saa3* levels. Analysis of global gene expression revealed perturbation of the same biological processes and pathways in liver, including the HMG-CoA reductase pathway. Both MWCNTs induced similar histological hepatic changes, with a tendency towards greater response following CNT_{Large} exposure.

Overall, we show that pulmonary exposure to two different MWCNTs induces similar systemic and hepatic responses, including changes in plasma APR, lipid composition, hepatic gene expression and liver morphology. The results link pulmonary exposure to MWCNTs with risk of cardiovascular disease.

Introduction

Cardiovascular disease (CVD), a broad term used for all diseases of the cardiovascular system, is the leading cause of death worldwide, being responsible for 3 in every 10 deaths in 2008 (World Health Organization et al., 2011). Retrospective and prospective epidemiological studies show that pulmonary exposure to respirable air particulates increases the risk of CVD (Chen and Nadziejko, 2005; Clancy et al., 2002; Dockery et al., 1993; Erdely et al., 2011a; Li et al., 2007; Mikkelsen et al., 2011; Pope et al., 1995, 2004). Recent increases in the development and use of nanomaterials will inevitably increase their presence in the environment and thus enhance the risk of human exposure. Concern has

Abbreviations: APR, Acute phase response; BET, Brunauer–Emmett–Teller; CNT, Carbon nanotube; CRP, C-Reactive protein; CVD, Cardiovascular disease; FDR, False discovery rate; GO, Gene ontology; HDL, High density lipoprotein; LDL, Low density lipoprotein; MWCNT, Multi-walled carbon nanotube; Nano-CB, Nano-carbon black; Nano-TiO_2, Nano-sized titanium dioxide; SAA, Serum amyloid A; SEM, Scanning electron microscopy; TEM, Transmission electron microscopy; VLDL, Very low density lipoprotein.

* Corresponding author at: National Research Centre for the Working Environment, Lersø Parkallé 105, DK-2100 Copenhagen, Denmark.

E-mail addresses: spo@nrcwe.dk (S.S. Poulsen), ats@nrcwe.dk (A.T. Saber), almo@food.dtu.dk (A. Mortensen), szarek@uwm.edu.pl (J. Szarek), dongmei.wu@hc-sc.gc.ca (D. Wu), andrew.williams@hc-sc.gc.ca (A. Williams), oa@ruc.dk (O. Andersen), nrj@nrcwe.dk (N.R. Jacobsen), carole.yauk@hc-sc.gc.ca (C.L. Yauk), hwa@nrcwe.dk (H. Wallin), sabina.halappanavar@hc-sc.gc.ca (S. Halappanavar), ubv@nrcwe.dk (U. Vogel).

http://dx.doi.org/10.1016/j.taap.2015.01.011

been raised that this exposure may lead to increased risk of CVD (Saber et al., 2014).

Several studies have linked pulmonary exposure to different types of multi-walled carbon nanotubes (MWCNTs) via inhalation, instillation or aspiration to lung inflammation, sustained interstitial fibrosis, and granuloma formation in rodents (Ma-Hock et al., 2009; Pauluhn, 2010a,b; Porter et al., 2010; Reddy et al., 2010; Wang et al., 2011; Poulsen et al., 2013). In addition, extrapulmonary effects, such as plaque progression in apoE knock-out mice, increased levels of acute phase response (APR) proteins in the serum, and adverse developmental effects in offspring, have been reported in mice following pulmonary exposure to CNTs (Li et al., 2007; Hougaard et al., 2013; Erdely et al., 2011b).

Systemic effects of MWCNTs may occur by direct translocation from the target tissue. Indeed, several studies have reported translocation of MWCNTs to different organs, suggesting that they are capable of crossing the air–blood barrier. For example, MWCNTs were found in the lymph nodes following instillation (Aiso et al., 2011), in the brain, kidney, heart and liver following inhalation (Mercer et al., 2013; Stapleton et al., 2012), and in the spleen, liver and bone marrow following pharyngeal aspiration (Czarny et al., 2014). It is also possible that secondary effects result from MWCNT-induced release of cytokines and APR proteins into the systemic circulation during pulmonary inflammation. Increased concentrations of plasma APR proteins have been reported by many epidemiological studies investigating the cardiovascular effects of air pollution (Lowe, 2001; Mezaki et al., 2003; Libby et al., 2010; Estabragh and Mamas, 2013; Pussinen et al., 2007). Increased APR has been recognized as an important risk factors for CVD (Ridker et al., 2000; Saber et al., 2013; Kaptoge et al., 2012; Taubes, 2002; Estabragh and Mamas, 2013; Rivera et al., 2013; Johnson et al., 2004; Pai et al., 2004; Saber et al., 2014).

The APR is characterized by changes in plasma levels of APR proteins, including C-reactive protein (CRP), serum amyloid A (SAA) and fibrinogen, and changes in cholesterol homeostasis following acute and chronic inflammatory states (Bourdon et al., 2012a; Gabay and Kushner, 1999). SAA is a family of conserved and highly homologous high density lipoprotein (HDL) apolipoproteins, which in mice are the predominant APR proteins (Meek et al., 1992). Several tissues, including the lungs, express the *Saa3* gene. The two other isoforms, *Saa1* and *Saa2*, are considered liver-specific but are also expressed in lungs (Bourdon et al., 2012a; Husain et al., 2013; Uhlar and Whitehead, 1999; Halappanavar et al., 2011; Halappanavar et al., 2014). The most studied APR protein in humans is CRP. Physiologically, the APR is a beneficial response to local or systemic disturbances (e.g. infections); however, a persistent chronic APR is suggested to alter blood lipids and cholesterol biosynthesis, thereby increasing the risk of developing CVD (Bourdon et al., 2012a; Lindhorst et al., 1997). In the circulation, SAA is primarily a part of HDL. During an APR the concentration of SAA can be induced over 1000-fold, whereby SAA replaces ApoA-1 as the major HDL protein. HDL-SAA is cleared faster from systemic circulation than regular HDL (Hoffman and Benditt, 1983; McGillicuddy et al., 2009; Salazar et al., 2000), and SAA remodeling of HDL impairs HDL's ability to serve as an acceptor for macrophage cholesterol efflux mediated through ABCA1. The consequences are retaining peripheral cholesterol, reduced cholesterol biliary excretion from liver (Artl et al., 2000; Banka et al., 1995; Lindhorst et al., 1997), and macrophage transformation into foam cells (Artl et al., 2000; Lee et al., 2013). Foam cells are a major component of the fatty streak observed during development of atherosclerosis, a multigenic, endothelial disease. Consistent with this, viral vector-mediated overexpression of *Saa1* in ApoE$^{-/-}$ mice leads to increased plaque progression (Dong et al., 2011). Interestingly, nano-sized titanium dioxide (nano-TiO_2) from the same batch increased both pulmonary APR in C57BL/6 mice (Halappanavar et al., 2011; Husain et al., 2013), and induced plaque progression in ApoE$^{-/-}$ mice (Mikkelsen et al., 2011) following pulmonary exposure, thus linking nanoparticle exposure to CVD.

We recently reported that intratracheal instillation of two MWCNTs, a short, entangled CNT_{Small} and a longer, thicker CNT_{Large}, caused similar increases in pulmonary inflammation and APR in mice, characterized by global mRNA changes, increased infiltration of inflammatory cells into the lung lumen and changes in the lung morphology (Poulsen et al., 2014). CNT_{Small} and CNT_{Large} were selected by the OECD Working Party on Manufactured Nanomaterials and are available at the EU Joint Research Centre. We chose these two based on their physicochemical differences. In the present study we explore changes in various CVD biomarkers and in hepatic gene expression in mice from the above mentioned study at 1, 3 and 28 days following intratracheal instillation of CNT_{Small} and CNT_{Large}.

Materials and methods

Materials. The two MWCNTs used in this study have been described previously (Poulsen et al., 2014). Briefly, the first MWCNT (NRCWE-026) is small and entangled, and was purchased from Nanocyl, Belgium. In this study NRCWE-026 will be referred to as CNT_{Small}. The other MWCNT (NM-401) was donated by the EU Joint Research Centre and is longer and thicker than CNT_{Small}. In this study it is referred to as CNT_{Large}, and it is physicochemically similar to Mitsui XNRi-7, which was recently classified as possibly carcinogenic to humans (Group 2B) by IARC (Grosse et al., 2014). Another batch of CNT_{Small} was donated to the EU Joint Research Centre repository; so both MWCNTs are included in the materials of the OECD Working Party on Manufactured Nanomaterials. The physicochemical characterization of CNT_{Small} and CNT_{Large}, including thermal gravimetric analyses (TGA), surface area analysis (BET), light microscopy imaging, scanning electron microscopy (SEM) imaging, transmission electron microscopy (TEM) imaging and elemental composition, has been conducted previously (Jackson et al., 2014; Kobler et al.,2015; Poulsen et al., 2014), and the data are summarized in the Results section.

Preparation of instillation medium and exposure stock. MWCNTs were suspended to a concentration of 3.24 mg/ml by sonication using a Branson Sonifier S-450D (Branson Ultrasonics Corp., Danbury, CT, USA) equipped with a disruptor horn (model number: 101-147-037) in NanoPure water containing 2% serum collected from C57BL/6 mice. Total sonication time was 16 min at 40 W with continuous cooling on ice. Vehicle controls contained NanoPure water with 2% serum and were sonicated as described for the MWCNT suspensions.

Animals, exposure and tissue collection. All handling, care taking and experimental procedures involving live animals have been reported previously (Kobler et al., 2014, 2015). Briefly, female C57BL/6 mice (6 per group) aged 5–7 weeks were allowed to acclimatize for 1–3 weeks before exposure. The mice were anesthetized with 4% isoflurane until fully relaxed and with 2.5% during the instillation. They were exposed to 18, 54 or 162 μg/animal of either CNT_{Small} or CNT_{Large} via a single intratracheal instillation. Intratracheal instillation was chosen since it allows for control of the deposited doses; this would be difficult with inhalation exposure. Although instillation bypasses the upper respiratory system and results in a rapid bolus deposition, it is a valuable tool for understanding the potential systemic toxicity following MWCNT exposure. Also, comparable inflammation levels following MWCNT administration by pharyngeal aspiration and by inhalation at a similar benchmark-deposited-dose have been demonstrated (Porter et al., 2013), indicating that non-inhalation administration may predict the response following inhalation. The doses used were selected for studying systemic and hepatic mechanisms following a pulmonary exposure to MWCNTs and they are within the dose ranges of other instillation/aspiration studies (Kim et al., 2014; Park et al., 2009; Porter et al., 2010; Shvedova et al., 2008; Snyder-Talkington et al., 2013). They correspond to 1, 3, and 9 days of exposure (8 h/day) to CNTs, assuming 33% deposition rate (Ma-Hock et al., 2009; Jackson

et al., 2011) and a ventilation rate of 1.8 l/h for mice, at the current Danish occupational exposure level for carbon black (3.5 mg/m^3). When considering the recommended exposure limit for CNTs of 1 μg/m^3 per 8 hour work shift (NIOSH, 2013), the lowest dose of 18 μg/mouse corresponds to the expected human work life exposure assuming a 10% deposition (Ma-Hock et al., 2009), a ventilation rate of 1.8 l/h, a 40 h working week and a 40 year work life. The dose of 56 μg corresponds to 3 times the life-long dose and 162 μg/mouse corresponds to 9 times the proposed life dose. Work place exposure to CNT are reported in the range of 10–300 μg/m^3 (Birch et al., 2011; Dahm et al., 2013; Erdely et al., 2013; Han et al., 2008; Lee et al., 2010; Maynard et al., 2004; Methner et al., 2010b, 2012), thus 10–300 times above the proposed exposure limit. At an air concentration of 10 μg/m^3, 162 μg/mouse would correspond to the total dose during a 40-year working life, whereas 162 μg/mouse corresponds to pulmonary deposition during 1.5 work years at 300 μg/m^3. Control animals were instilled with vehicle (NanoPure water with 2% serum). The mice were euthanized1, 3 or 28 days after exposure by exsanguination via intracardiac puncture. Immediately after withdrawal of the heart blood (800–1000 μl), liver tissue was collected and samples were snap-frozen in cryotubes in liquid N_2 and stored at −80 °C. Whole blood was fractionated by centrifugation and plasma was collected and stored at −80 °C. Additional liver specimens were taken from 12 to 24 vehicle control mice and from 5 to 6 mice from groups treated with either CNT_{Small} or CNT_{Large}. Tissues were fixed in 4% neutral buffered formaldehyde, paraffin-embedded and sections 4–6 μm thick were stained with hematoxylin and eosin (HE) for histological examination.

All animal procedures followed the guidelines for the care and handling of laboratory animals established by Danish law. The Animal Experiment Inspectorate under the Ministry of Justice approved the study (#2010/561-1779).

Plasma protein measurements. ELISA analysis specifically targeting plasma SAA3 levels was conducted in accordance with the manufacturer's instructions (Mouse Serum Amyloid A-3, Cat.#EZMSAA3-12K, Millipore). All of the time points and doses were evaluated. Samples were pooled to a final N of 3 per group (representing 6 mouse samples in total). Plasma haptoglobin was determined by ELISA (mouse haptoglobin (Hpt/HP) ELISA kit, Cat. #CSB-E08586m, Cusabio) as described by the manufacturer. The high dose only from all time points was evaluated. The samples were pooled to a final N of 3 per group.

The statistical analyses were performed in SAS version 9.3 (SAS Institute Inc., Cary, NC, USA). Statistical significance was calculated using a parametric two-way ANOVA with a post-hoc Tukey-type experimental comparison test. In case of interaction between dose and time, the data were separated in time points and a one-way ANOVA with a post-hoc Tukey-type experimental comparison test was performed. For the statistical analysis of haptoglobin protein levels, no statistically significant time-variance between controls was found; thus, controls from all time points were pooled.

Plasma lipid composition. Plasma levels of total cholesterol, HDL and low-density lipoprotein/very low-density lipoprotein (LDL/VLDL) in mice exposed to CNT_{Small} and CNT_{Large} were determined colorimetrically with the EnzyChrom™ AF HDL and LDL/VLDL assay kit (EHDL-100, BioAssay Systems) according to the manufacturer's instructions. All time points and doses were evaluated with 6 animals per treatment group. Briefly, a standard sample was produced from a standard cholesterol reference supplied by the manufacturer. HDL was isolated from the supernatant following centrifugation of a 1:1 plasma-precipitating reagent solution. The LDL/VLDL fraction was separated by dissolution of the collected pellet from the 1:1 plasma-precipitating reagent solution in PBS. Plasma cholesterol, HDL, and LDL/VLDL isolations from each sample and a standard cholesterol reference supplied by the manufacturer were placed in 50 μl aliquots as duplicates in a 96-well plate. Sixty microliters of a NAD-enzyme buffer mix was added, and the plate was incubated at room temperature for 30 min. Fluorescence measurements were recorded on Victor^2 1420 Multi label counter (Wallac, Perkin-Elmer) at OD 340 nm and cholesterol concentrations were determined by comparison to the standard sample.

Plasma triglyceride levels were determined using the EnzyChrom™ AF Triglyceride assay kit (BioAssay Systems, ETGA-200) according to the manufacturer's instructions. All time points and doses were evaluated. There were 6 animals per treatment group. Briefly, a 10-fold serial diluted standard curve was produced from a standard cholesterol reference supplied by the manufacturer. Ten microliter aliquots of standard and sample were placed in duplicate in a 96-well plate, and 100 μl of a dye reagent-enzyme mix was added. The plate was incubated at room temperature for 30 min. The color intensity of the reaction product was determined spectrophotometrically at OD 570 nm on a Victor^2 1420 Multi label counter (Wallac, Perkin-Elmer), and total triglyceride concentrations were determined by a standard curve.

All statistical analyses on lipid levels were performed in SAS version 9.2 (SAS Institute Inc., Cary, NC, USA). Statistical significance was calculated using a parametric one-way ANOVA with a post-hoc Tukey-type experimental comparison test.

Total lipid extraction and total hepatic cholesterol analysis. Total lipids were extracted from liver tissue according to the Folch method (Folch et al., 1957). In brief, approximately 4–5 mg of liver tissue was collected from the sample and the weight was noted. The liver tissue was homogenized in 250 μl methanol and 250 μl water. A double volume of 5:1 chloroform/methanol was then added, and phases were separated by centrifugation. The lower layer containing chloroform/lipid was collected, and the chloroform removed under nitrogen gas flow. Lipids were resuspended in 100 μl EnzyChrom assay buffer and stored at −20 °C until analysis.

Colorimetric quantification of hepatic cholesterol levels was determined with the EnzyChrom™ AF Cholesterol assay kit (BioAssay Systems, E2CH-100) according to the manufacturer's instructions. All time points and doses were evaluated with 6 animals per treatment group. Briefly, a 10-fold serial diluted standard curve was produced from a standard cholesterol reference supplied by the manufacturer. Fifty microliter aliquots of standard and sample were placed in duplicate in a 96-well plate, and 50 μl of a dye reagent–enzyme mix was added. The plate was incubated at room temperature for 30 min. The color intensity of the reaction product was spectrophotometrically measured at OD 570 nm on a Victor^2 1420 Multi label counter (Wallac, Perkin-Elmer), and total cholesterol concentrations were determined by comparison to the standard curve, with normalization to extracted tissue weight.

Total RNA extraction. Total RNA was isolated from liver tissue of 144 mice in total (N was 6 mice per dose group and time point). The RNA was isolated using TRIzol reagent (Invitrogen, Carlsbad, CA, USA) and purified using RNeasy MiniKits (Qiagen, Mississauga, ON, Canada) as described by the manufacturer. On-column DNase treatment was applied (Qiagen, Mississauga, ON, Canada). All RNA samples showing A260/280 ratios between 2.0 and 2.15 were further analyzed for RNA integrity using an Agilent 2100 Bioanalyzer (Agilent Technologies, Mississauga, ON, Canada). RNA integrity numbers above 7.0 were used in the experiment. If the RNA samples did not fulfill the criteria, new RNA extractions from the liver tissue were performed. Total RNA was stored at −80 °C until analysis.

Microarray hybridization. We have found changed hepatic gene expression only after pulmonary exposure to high doses of nano-TiO_2 or nano-carbon black (nano-CB) (Bourdon et al., 2012a; Husain et al., 2013). Therefore, microarray analysis was done only for the 0 and 162 μg dose groups in this study. The two lower doses (18 and 54 μg) were included for time points 1 and 3 days in the subsequent RT-PCR confirmation of the microarray results. A total of 200 ng of RNA from

each sample (6 per treatment group) was analyzed by microarray hybridization on Agilent 8 × 60 K oligonucleotide microarrays (Agilent Technologies Inc., Mississauga, ON, Canada) as described previously (Poulsen et al., 2013). Data were acquired using Agilent Feature Extraction software version 9.5.3.1.

Statistical, functional and pathway analysis of microarray data. The microarray data were analyzed as described previously (Poulsen et al., 2013, 2014). Genes showing expression changes of at least 1.5-fold in either direction compared to their matched controls and having false discovery rate adjusted p-values of less than or equal to 0.05 (FDR $p \leq 0.05$) were considered significantly differentially expressed and were used in the downstream analysis. We used the Database for Annotation, Visualization and Integrated Discovery (DAVID) v6.7 and Ingenuity Pathway Analysis (IPA, Ingenuity Systems, Redwood City, CA, USA) for functional and pathway analyses, as previously described (Poulsen et al., 2014). The gene ontology (GO) classification of the differentially expressed genes was explored; GO consists of three structured controlled vocabularies (ontologies) that describe gene products in terms of their associated biological processes, cellular components and molecular functions in a species-independent manner. In the present study GO biological processes were utilized.

qRT-PCR validation. Eighteen genes were selected for further validation by qRT-PCR in liver tissue using custom RT^2 Profiler PCR Arrays and a BioRad CFX96 real-time PCR detection system at doses 0, 18, 54 and 162 μg for post-exposure days 1 and 3, and at doses 0 and 162 μg at post-exposure day 28. The selected differentially expressed genes (FDR $p \leq 0.05$, FC 1.5 in at least one condition) showed large changes in expression following MWCNT exposure, and/or were associated with lipid homeostasis, or inflammatory and acute phase responses. A custom RT^2 Profiler PCR Array plate, the RT^2 First Strand Kit and RT^2 SYBR® Green qPCR Mastermix (QIAGEN Sciences, Maryland, USA) was used. Hypoxanthine-guanine phosphoribosyltransferase (*Hprt*), actin β (*Actb*) and glyceraldehyde 3-phosphate dehydrogenase (*Gapdh*) were used as reference genes for normalization and were selected based on their stable expression levels in the treated and control samples in the microarray analysis. A threshold value was set to 10^2. The final qRT-PCR validation group consisted of a sample size of 3 per treatment condition.

Results

MWCNT

Detailed physicochemical characterization of the materials has been published elsewhere (Kobler et al., 2014; Jackson et al., 2014; Kobler et al., 2015; Poulsen et al., 2014). In brief, CNT_{Small} were 847 ± 102 nm long and 11 (6–17) nm wide. They contained 87% carbon and had a BET surface area of 245.8 m^2/g. A chemical analysis of CNT_{Small} from the same batch showed that main components of CNT_{Small} (NRCWE-026) included the following: C (84.4%), Al_2O_3 (14.97%), Fe_2O_3 (0.29%) and CoO (0.11%) (Jackson et al., 2014). CNT_{Small} appeared curly and highly entangled when visualized by TEM and SEM. CNT_{Large} were 4048 ± 366 nm in length and had an average width of 67 (24–138) nm. CNT_{Large} consisted of 97% carbon and the BET surface area was 14.6 m^2/g. The chemical composition of CNT_{Large} from the same batch showed that the main components of CNT_{Large} (NM-401) included the following: C (99.7%), P_2O_5 (0.14%), CO_3 (0.08%) and Fe_2O_3 (0.05%) (Jackson et al., 2014). CNT_{Large} appeared large and straight when visualized by TEM and SEM.

Plasma protein analysis

Plasma levels of SAA3 were statistically significantly increased in mice exposed to both types of MWCNTs. This was observed following CNT_{Small} exposure in the high dose group on post-exposure day 1 and day 28, and at all doses on post-exposure day 3 (4.3-, 7.0-, 2.5-, 10.4-, and 32.8-fold increase, respectively) (Fig. 1A). CNT_{Large} exposure resulted in increased SAA3 levels following high dose exposure on day 1, and at the medium and high dose on post-exposure day 3 (6.9, 3.2 and 61.0 fold increase, respectively) (Fig. 1A). There were no changes at 28 days after CNT_{Large} exposure. One observation in the control group on day 28 was an outlier (more than 2 SD difference from the other values), resulting in a relatively high control SAA3 plasma protein content. If this observation was excluded, the difference was statistically significant for both medium and high dose exposures 28 days post-exposure. Interestingly, we observed large increases in pulmonary *Saa3* mRNA levels in the same animals after pulmonary exposure to CNT_{Small} and CNT_{Large} (Poulsen et al., 2014). Pulmonary *Saa3* mRNA levels correlated strongly with SAA3 protein levels in the plasma (Fig. 1B) (linear regression; $p < 0.0005$ across time points and MWCNT dose). The haptoglobin plasma levels were statistically significantly increased 3 days after exposure to 162 μg CNT_{Small} and CNT_{Large} compared to vehicle controls (Fig. 1C), but were not changed at other time points.

Alterations in cholesterol homeostasis

Compared to the controls, total cholesterol levels were greatly increased after exposure to either type of MWCNT on day 3 at the high dose (58% and 51% for CNT_{Small} and CNT_{Large}, respectively) (Fig. 2A) and on post-exposure day 1 for CNT_{Large} (28%). Significantly higher LDL/VLDL plasma levels were found for the high dose 3 days post-exposure groups for both MWCNTs (153% and 128% for CNT_{Small} and CNT_{Large} respectively) (Fig. 2B). HDL levels were increased following high dose exposure to CNT_{Small} on day 3 (42%). A similar but statistically non-significant increase was observed for CNT_{Large} under the same exposure conditions (31%) (Fig. 2C). The ratios between plasma HDL and LDL/VLDL levels in the controls (CNT_{Small}: 3.56, CNT_{Large}: 3.22) compared to the high dose exposed mice at day 3 (CNT_{Small}: 1.92, CNT_{Large}: 1.94) showed that the increase in the LDL/VLDL level was greater than the increase in HDL following exposure. Plasma triglyceride levels were unaffected by CNT_{Small} and CNT_{Large} exposure (results not shown).

No change in total hepatic cholesterol levels was observed for CNT_{Small}, but a statistically significant 47% increase was observed for CNT_{Large} on post-exposure day 3 (Fig. 2D).

Microarray analysis

The experiments and analyses adhered to MIAME standards (Edgar and Barrett, 2006). All microarray data have been deposited in the NCBI Gene Expression Omnibus database and can be accessed through the accession number GSE61366.

Alterations in global hepatic gene expression

Global hepatic gene expression was assessed for the highest dose of both MWCNT exposures for all three time points. For CNT_{Small} exposed mice, a total of 4028 of the 60,000 probes were differentially expressed in hepatic tissue. On day 1, day 3 and day 28 the expression of 2505, 2401, and 255 genes, respectively, was changed (Supplementary Table 1). Fig. 3A shows the overlap of differentially expressed genes across time points. CNT_{Large} had a slightly smaller effect on hepatic gene expression than CNT_{Small} exposed mice, but still caused a significant effect; a total of 3089 probes were differentially expressed compared to controls. On day 1, the expression of 2128 genes was changed, and on day 3, 1667 gene expressions were altered. No genes were significantly differentially expressed on day 28. As observed after exposure to CNT_{Small}, many of the same genes were differentially expressed on day 1 and day 3 (Fig. 3B).

GO classification analysis in DAVID (Huang et al., 2009a,b) revealed statistically significant perturbations in biological processes in the liver at the early time points (day 1 and 3) only. The common GO biological

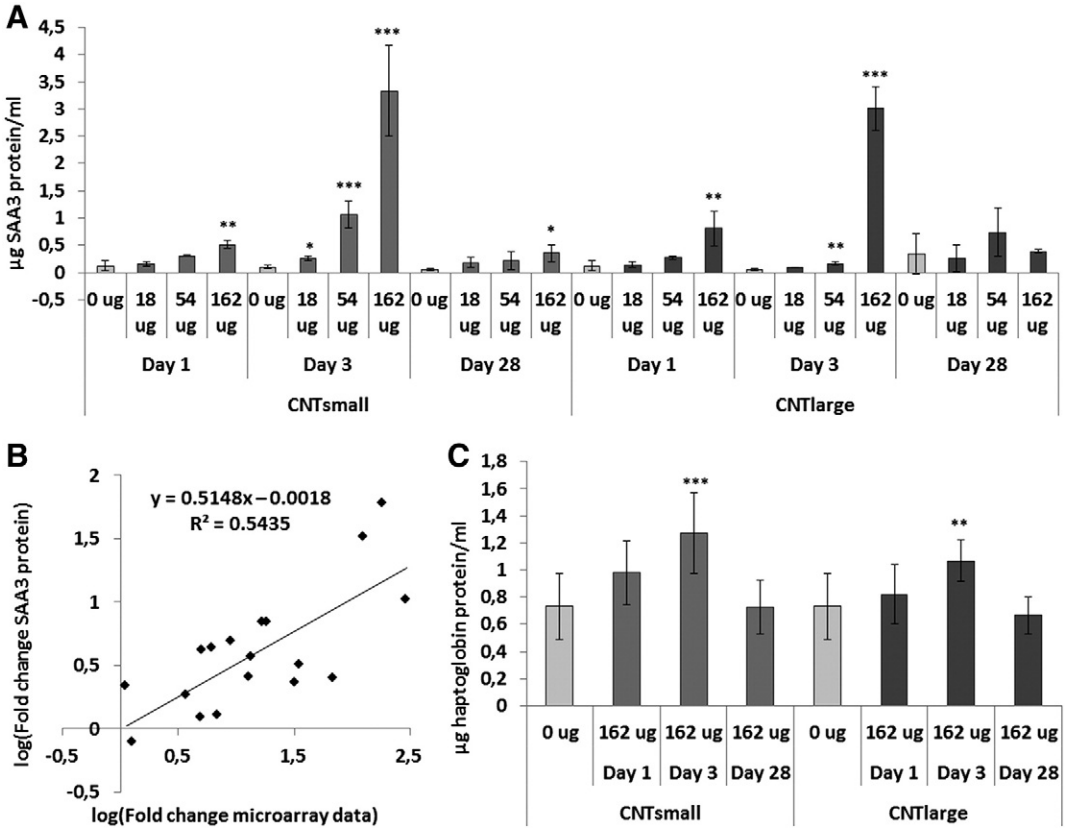

Fig. 1. Plasma protein levels of SAA3 and haptoglobin following exposure to CNT_{Small} or CNT_{Large}. (A) Plasma levels of SAA3 protein following intratracheal instillation of 0, 18, 54 or 162 µg CNT_{Small} or CNT_{Large} at post-exposure day 1, 3 or 28. (B) Linear regression analysis of pulmonary *Saa3* mRNA fold changes after microarray analysis and plasma SAA3 protein fold changes following ELISA analysis. Both microarray and protein level data have been log transformed. (C) Plasma levels of haptoglobin protein following intratracheal instillation of 0 or 162 µg CNT_{Small} or CNT_{Large} at post-exposure day 1, 3 or 28. *Statistically significantly different from vehicle instilled mice, $p < 0.05$. **Statistically significantly different from vehicle instilled mice, $p < 0.01$. ***Statistically significantly different from vehicle instilled mice, $p < 0.001$. Error bars denote SD.

processes affected following CNT_{Small} and CNT_{Large} exposure are shown in Fig. 3C. We observed a high degree of concordance between the two MWCNTs for enriched GO biological processes, especially for oxidation reduction [GO:0055114], steroid metabolic process [GO:0008202], lipid biosynthetic process [GO:0008610], fatty acid metabolic process [GO:0006631], cofactor metabolic process [GO:0051186] and immune response [GO:0006955], which were differentially enriched both 1 and 3 days following CNT_{Small} and CNT_{Large} exposure. The uniquely differentially regulated biological processes are shown in Supplementary Table 2 and revealed few major differences. Several of the highly enriched processes in common for the two MWCNTs were associated with lipid homeostasis. Remarkably similar and pronounced effects on gene expression for both MWCNTs were observed by functional annotation clustering (Supplementary Table 3), where lipid metabolic process was the top scoring cluster at the early time points. Across both MWCNT types at the early points, oxidation reduction [GO:0055114] was the most enriched regulated biological process. Several of the differentially regulated genes under this process were involved in other biological processes as well, including lipid homeostasis processes.

IPA was employed to relate the functional significance of the GO changes to biological functions and pathways. The individual enriched functions in IPA were filtered by 1) removing redundant functions with overlapping genes, and 2) removing functions that were not directly relevant to the present study (e.g. renal diseases, ophthalmic diseases etc.). By using these criteria, we identified the top 5 most significantly affected functions after CNT_{Large} exposure, and we compared these to the corresponding functions following CNT_{Small} exposure (Supplementary Fig. 1). The top-regulated functions were similar for both MWCNTs, with 3 out of 5 of the most regulated functions being the same. 'Lipid metabolism' was the most enriched function, in agreement with the observed changes in the GO biological processes involving lipid homeostasis. The third most perturbed function after CNT_{Small} exposure was 'cardiovascular disease', and the fifth was 'carbohydrate metabolism'.

Inflammation and acute phase response signaling

Inflammatory processes were among the most perturbed processes in the liver. These were in part driven by changes in the mRNA levels of several cytokines, including the following: *Cxcl1*, *Cxcl9*, *Cxcl10*, *Cxcl13*, *Ccl6*, *Ccl27a* and *Ccl25*. We also found differential expression of APR genes in the liver following MWCNT exposure including the following: *Saa1*, *Saa2*, *Saa3*, *Saa4*, *Orm1*, *Orm2*, *Orm3*, *Mt1* and *Mt2* (Supplementary Table 4). As recently reported, strong pulmonary inflammatory and APR, both as increased neutrophil influx and increased expression of cytokines and APR genes, were found in these mice following same exposure to CNT_{Small} and CNT_{Large} (Poulsen et al., 2014).

Regulation of cholesterol homeostasis

Analysis of the global hepatic gene expression revealed consistent perturbation of lipid homeostasis related functions and pathways. Genes involved in the HMG-CoA reductase pathway were substantially down-regulated in the liver for both MWCNTs, which is consistent with perturbations in lipid processes identified using DAVID (Fig. 3C) and functional analysis in IPA (Supplementary Fig. 1 and Supplementary Table 3). CNT_{Small} was the most effective in perturbing the HMG-CoA reductase pathway (*Hmgcr*, *Mvk*, *Pmvk*, *Mvd*, *Fdps*, *Sqs*, *Sqle*, *Dhcr7*) in the liver. The changes in gene expression were similar on days 1 and 3 (Table 1). In addition to the HMG-CoA reductase pathway, other genes

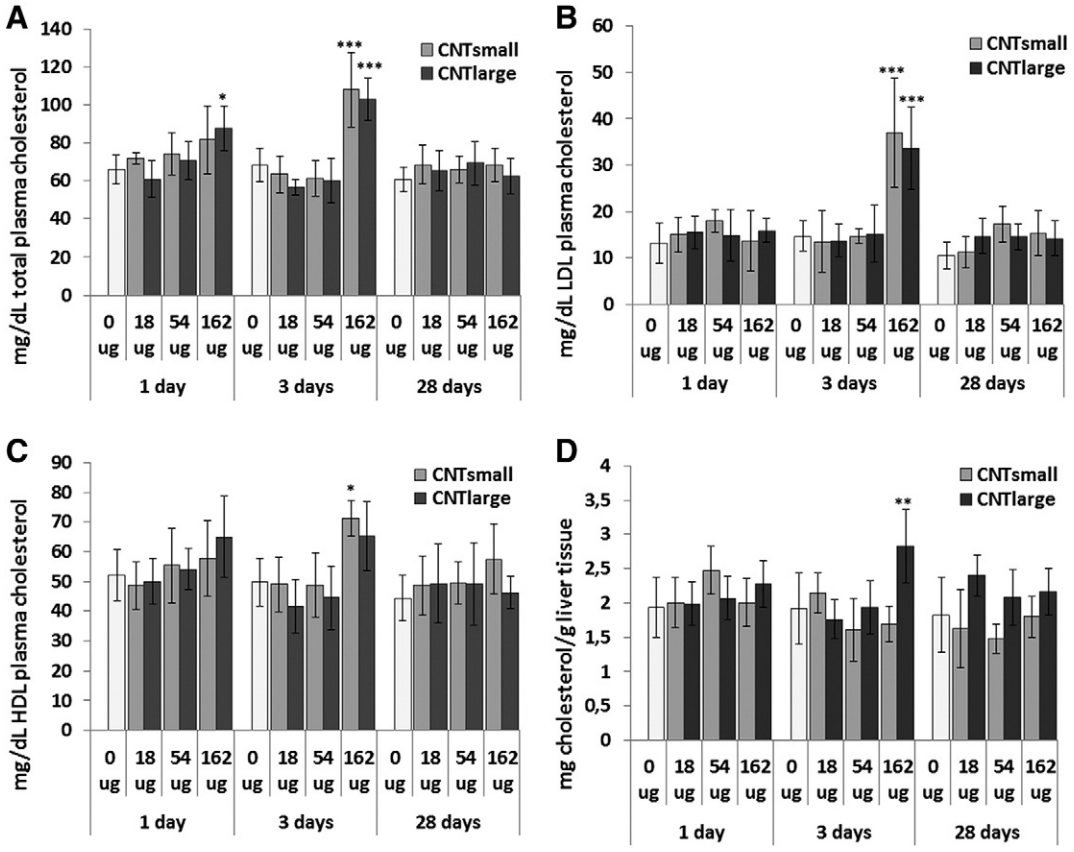

Fig. 2. Changes in plasma and hepatic cholesterol levels following exposure to CNT_{Small} or CNT_{Large}. (A) Plasma total cholesterol, (B) plasma LDL, (C) plasma HDL and (D) hepatic total cholesterol in C57BL/6 mice exposed to 0, 18, 54 or 162 μg CNT_{Small} or CNT_{Large} at post-exposure day 1, 3 or 28. *Statistically significantly different from vehicle instilled mice, $p < 0.05$. **Statistically significantly different from vehicle instilled mice, $p < 0.01$. ***Statistically significantly different from vehicle instilled mice, $p < 0.001$. Error bars denote SD.

involved in lipid homeostasis were also affected by MWCNT exposure. Low density lipoprotein receptor (*Ldlr*) was down-regulated after CNT_{Small} exposure on day 1 (−1.79-fold) and day 3 (−1.7-fold), and after CNT_{Large} exposure at day 3 (−1.56-fold) (Table 1). Gene expression of another membrane protein, scavenger receptor class B, member 1 (*Scarb1*), was also down-regulated for CNT_{Small} day 1 (−1.53-fold), whereas expression of low density lipoprotein receptor-related protein 1 (*Lrp1*) was up-regulated on day 3 for both MWCNTs (CNT_{Small} 1.84-fold, CNT_{Large} 2.09-fold). *Scarb1* and *Lrp1* are involved in the transport of HDL and LDL, respectively, over the hepatocyte cell membrane. A small up-regulation in the expression of *Abca1* was identified 3 days post-exposure for CNT_{Small} (1.68-fold).

Besides the HMG-CoA reductase pathway, analysis of canonical pathways in IPA (Supplementary Fig. 2) also revealed enrichment of LXL/RXR activation, glutathione-mediated detoxification, acute phase response signaling, nicotine degradation III, hepatic cholestasis and xenobiotic metabolism signaling pathways. Analysis of the LXL/RXR activation pathway on day 3 for both MWCNTs revealed that most upstream and downstream genes related to the LXL/RXR heterodimer complex show changes in expression (Supplementary Fig. 3), including cholesterol transporter *Abca1*. As observed for the HMG-CoA pathway, CNT_{Small} exposure induced the largest change in gene expression of genes in this pathway.

qRT-PCR validation

We validated 18 differentially expressed genes in liver tissue following pulmonary exposure to 162 μg CNT_{Small} or CNT_{Large} at post-exposure day 1, 3 or 28. These genes were chosen due to their involvement in lipid homeostasis (*Hmgcr*, *Pmvk*, *Mvd*, *Fdps*, *Dhcr7*, *Ldlr*, *Lrp1*, *Cyp7a1*, *Abca1*), inflammatory and APR (*Cxcl1*, *S100a9*, *Saa1*, *Saa2*, *Saa3*, *Il1r1*) or due to large changes in their expression following MWCNT exposure (*Sult1e1*, *Scd1*, *Dbp*). In addition to this validation, we evaluated the 18 and 54 μg exposure groups on post-exposure days 1 and 3 in order to assess hepatic changes following lower dose MWCNT exposure. The qRT-PCR results are provided in Table 2 and are consistent with the DNA microarray results. The lipid homeostasis genes *Hmgcr*, *Ldlr* and *Cyp7a1* were differentially expressed at all doses on days 3 and 28 after CNT_{Small} exposure, but not following CNT_{Large} exposure. In contrast, there was a tendency towards greater enrichment of inflammatory and APR genes following exposure to CNT_{Large} compared to CNT_{Small}. The expression of *Dbp*, a PAR leucine zipper transcription factor involved in circadian rhythm regulation, was consistently down-regulated at all doses and time points following exposure to CNT_{Small}, whereas CNT_{Large} exposure resulted in up-regulation of the expression at the high and medium dose on post-exposure day 1.

Liver histology

Different doses of CNT_{Small} or CNT_{Large} induced histological changes in the liver at different times (Fig. 4 and Supplementary Table 5) with no apparent dose- or time-dependence. No translocation of MWCNTs from lungs to liver was observed. Changes such as vacuolar degeneration (Figs. 4C–J), granulomas (Figs. 4C and G–J), necrosis of hepatocytes (Figs. 4D and I–J), increased number and/or hypertrophy of Kupffer cells (Figs. 4A and I–J) were frequent in CNT-treated mice. For both MWCNT types the incidence of lesions was higher 3 and 28 days after exposure than on post-exposure day 1. The sites of vacuolar degeneration in the cytoplasm of hepatocytes within the hepatic lobule differed between CNT_{Small} and CNT_{Large} exposure. Whereas the vacuolar degeneration

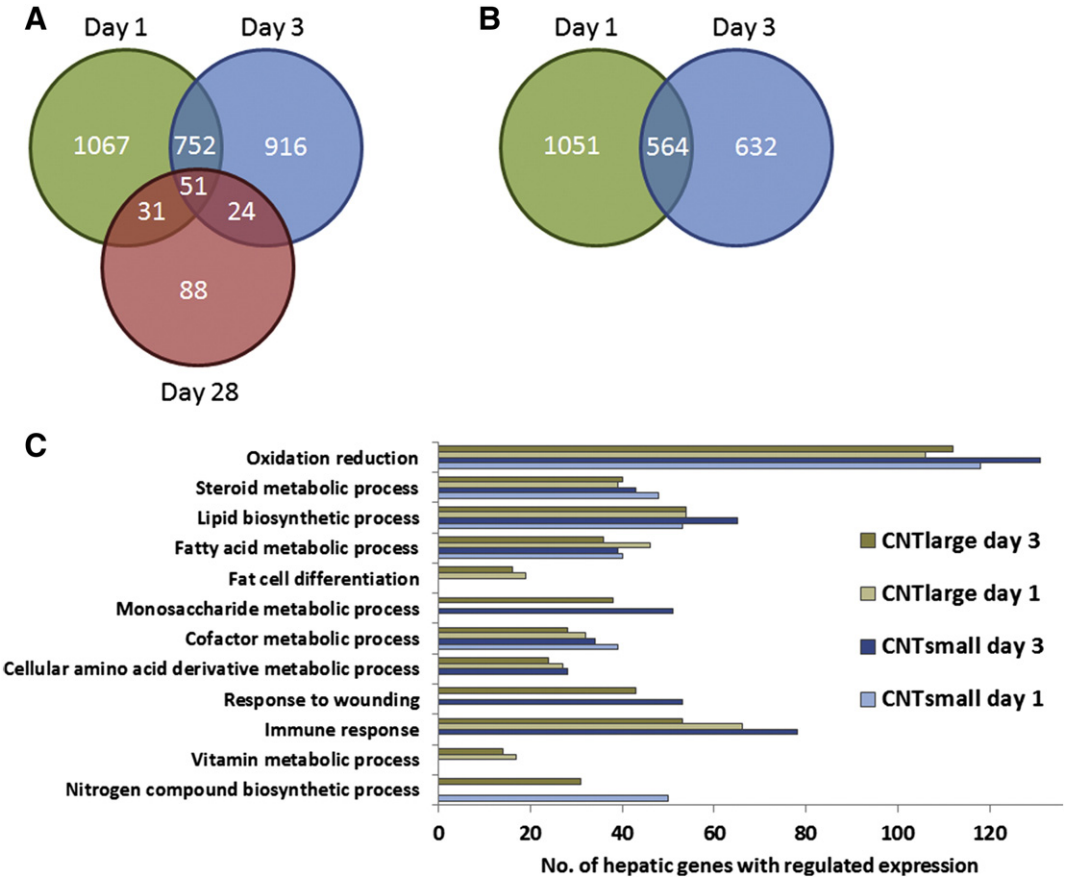

Fig. 3. Hepatic transcriptomic changes. (A) Venn diagram of differentially expressed genes following exposure to 162 μg CNT_{Small}. $p < 0.05$ and fold change ±1.5. (B) Venn diagram of differentially expressed genes following exposure to 162 μg CNT_{Large}. $p < 0.05$ and fold change ±1.5. (C) Changes in GO biological processes in the liver following exposure to CNT_{Small} and CNT_{Large}. Determined through DAVID Bioinformatics Resources 6.7.

after CNT_{Large} exposure was distributed throughout the whole area of the hepatic lobule regardless of the time after instillation, after CNT_{Small} exposure it was located in the centrilobular zone (i.e. near the central vein) 1 day after exposure, mid-zonal three days after exposure and in the periportal zone 28 days after exposure. Although liver granulomas were observed after exposure to both MWCNTs, they were larger and more frequent following CNT_{Large} exposure (Figs. 4C and G–J). Microfoci of necrosis, eosinophilic necrosis and hepatocytes with pyknotic nuclei were seen following exposure to either MWCNT and were located close to granulomas; however, they were more frequent after CNT_{Large} exposure. Eosinophilic necrotic hepatocytes surrounding the central vein were observed in the livers of mice 1 or 3 days after exposure to 162 μg CNT_{Large}. Increased number and hypertrophy of Kupffer cells were observed more frequently in livers from mice exposed to CNT_{Large} (Figs. 4D and I–J). Binucleate hepatocytes were more frequent in the livers of exposed mice than in the controls. Overall, pulmonary exposure to CNT_{Large} was associated with increased incidence and severity of morphological liver lesions compared to exposure to CNT_{Small}.

Table 1
Differentially expressed hepatic genes involved in lipid metabolism processes following exposure to CNT_{Small} or CNT_{Large}.

Gene name	CNT_{Small}						CNT_{Large}					
	Day 1		Day 3		Day 28		Day 1		Day 3		Day 28	
	FC	p-Value	FC	p-Value	FC	p-Value	FC	p-Value	FC	p-Value	FC	p-Value
HMG-CoA reductase (HMGCR)	−2.18	0.013	−3.0	0.001	–	–	–	–	−2.63	0.005	–	–
Mevalonate kinase (MVK)	−1.98	0.006	–	–	–	–	–	–	–	–	–	–
Phosphomevalonate kinase (PMVK)	−3.05	0.0	−1.75	0.001	–	–	−2.27	0.0	−2.66	0.0	–	–
Mevalonate-5-pyrophosphate (MVD)	–	–	−2.22	0.012	–	–	–	–	−2.93	0.001	–	–
Farnesyl-PP synthase (FDPS)	−2.31	0.000	−1.89	0.017	–	–	−2.67	0.0	−3.16	0.0	–	–
Squalene synthase (SQS)	−1.75	0.009	–	–	–	–	–	–	–	–	–	–
Squalene epoxydase (SQLE)	−2.05	0.025	–	–	–	–	–	–	–	–	–	–
7-Dehydrocholesterol reductase (DHCR7)	−2.22	0.0	−1.99	0.0	–	–	−2.09	0.0	−2.33	0.0	–	–
Low density lipoprotein receptor (LDLR)	−1.79	0.002	−1.70	0.006	–	–	–	–	−1.56	0.041	–	–
Low density lipoprotein receptor-related protein 1 (LRP1)	–	–	1.84	0.0	–	–	–	–	2.09	0.0	–	–
Scavenger receptor class B, member 1 (SCARB1)	−1.53	0.0	–	–	–	–	–	–	–	–	–	–
Cytochrome P450, family 7, subfamily a, polypeptide 1 (CYP7A1)	–	–	−20.16	0.0	–	–	–	–	−4.0	0.007	–	–
Hepatic lipase (LIPC)	–	–	−1.50	0.002	–	–	–	–	–	–	–	–
ATP-binding cassette, sub-family A, member 1 (ABCA1)	–	–	1.68	0.0	–	–	–	–	–	–	–	–

FC: Fold change. –: Not significantly differentially expressed. Numbers are statistically significant at least at the $p < 0.05$ level.

Table 2
Hepatic mRNA expression changes for selected genes in mice 1, 3 and 28 days post-exposure to 18 μg, 54 μg and 162 μg CNT.

CNT_{Small}	Day 1				Day 3				Day 28	
	PCR array			Microarray	PCR array			Microarray	PCR array	Microarray
Genes	18 μg	54 μg	162 μg	162 μg	18 μg	54 μg	162 μg	162 μg	162 μg	162 μg
Sult1e1	–	–	51.3	42.2	–	–	58.6	27.3	–	–
Scd1	−2.5	−2.3	−2.5	–	–	–	−227.5	−47.1	–	–
Cxcl1	–	–	–	–	–	–	63.3	18.6	–	–
S100a9	–	–	–	2.4	–	–	17.1	12.2	–	–
Saa1	–	–	–	2.6	1.8	4.7	–	8.2	–	–
Saa2	–	–	–	–	–	–	–	6.1	–	–
Saa3	–	–	–	–	–	–	–	2.2	–	–
Il1r1	–	–	3.5	5.2	−1.8	–	18.1	10.1	–	–
Hmgcr	−2.4	–	–	−2.2	−3.4	−3.4	−4.5	−3.0	−3.4	–
Pmvk	–	–	−2.9	−3.1	–	–	–	−1.8	–	–
Mvd	–	–	–	–	–	–	−3.0	−2.2	−2.6	–
Fdps	–	–	−2.5	−2.3	–	–	–	−1.9	–	–
Dhcr7	–	–	−2.0	−2.2	–	–	–	−2.0	–	–
Ldlr	−2.1	–	−1.5	−1.8	−2.4	−2.2	−2.5	−1.7	−2.0	–
Lrp1	–	–	–	–	–	–	1.9	1.8	–	–
Cyp7a1	−23.3	–	–	–	−6.6	−3.8	−39.3	−20.2	−2.1	–
Abca1	–	1.5	–	–	–	–	–	1.7	–	–
Dbp	−26.1	−4.6	−4.0	−7.9	−33.8	−11.0	−7.7	−10.1	−22.7	−12.3
CNT_{Large}	Day 1				Day 3				Day 28	
	PCR array			Microarray	PCR array			Microarray	PCR array	Microarray
Genes	18 μg	54 μg	162 μg	162 μg	18 μg	54 μg	162 μg	162 μg	162 μg	162 μg
Sult1e1	–	–	172.6	34.7	–	–	28.3	11.5	–	–
Scd1	–	–	−1.9	−1.8	–	–	−111.9	−52.4	–	–
Cxcl1	–	–	–	3.6	–	–	72.2	14.1	–	–
S100a9	–	–	4.4	2.4	–	–	7.7	4.1	–	–
Saa1	–	10.4	–	3.0	–	–	3839.4	9.1	–	–
Saa2	–	10.6	–	2.8	2.4	–	2521.4	8.2	–	–
Saa3	–	–	–	–	–	–	9.5	3.2	–	–
Il1r1	1.6	–	8.7	5.9	–	–	10.9	4.4	–	–
Hmgcr	–	–	–	–	–	–	–	−2.6	–	–
Pmvk	–	–	–	−2.3	–	–	−2.0	−2.7	–	–
Mvd	–	–	–	–	–	–	−2.5	−2.9	–	–
Fdps	–	–	–	−2.7	–	–	−2.3	−3.2	–	–
Dhcr7	–	–	–	−2.1	–	–	−2.2	−2.3	–	–
Ldlr	–	–	–	–	–	–	–	−1.6	–	–
Lrp1	–	–	–	–	–	–	2.7	2.1	–	–
Cyp7a1	–	–	–	–	–	–	–	−4.0	–	–
Abca1	–	–	–	–	–	–	2.2	–	–	–
Dbp	–	11.7	5.4	–	–	–	–	–	–	–

Fold change compared to vehicle instilled control mice. –: Not significantly differentially expressed. Numbers are statistically significant at least at the $p < 0.05$ level.

Discussion

In this study we investigated extrapulmonary effects in female C57BL/6 mice 1, 3 or 28 days following a single, intratracheal instillation of either of two MWCNTs with very different physicochemical properties. We report increased plasma levels of the APR protein haptoglobin and a large, sustained increase in plasma SAA3 protein levels following exposure to both types of MWCNTs. Systemic increases in haptoglobin and SAA levels have been observed previously following pulmonary CNT exposure (Erdely et al., 2011b; Saber et al., 2013), with increased SAA3 levels being detected up to one year post-exposure in male mice (Kim et al., 2014). We recently reported that CNT_{Small} and CNT_{Large} exposures, despite physicochemical fiber dissimilarities, elicit very similar, strong pulmonary inflammation and APR (Poulsen et al., 2014). This pulmonary APR was characterized by time- and dose-dependent increases in the expression of a number of acute phase genes, with *Saa3* being the most differentially expressed gene. We have previously reported similar findings for other nanomaterials and particles (Saber et al., 2014). In the present study, we observed a strong and statistically significant linear relationship between the pulmonary *Saa3* mRNA levels and SAA3 plasma levels (Fig. 1B), indicating a probable pulmonary origin of plasma SAA3. The hepatic expression levels of *Saa3* following CNT_{Small} and CNT_{Large} exposure were 10 to 100 times lower than the expression levels of pulmonary *Saa3*, thus indicating that the observed systemic APR may be a secondary response to the pulmonary APR induced by MWCNTs. This is in agreement with previous reports showing that pulmonary exposure to CB, diesel exhaust particle and MWCNTs induced little or no hepatic APR, but a large pulmonary APR (up to a 600-fold increase) (Bourdon et al., 2012a,b; Saber et al., 2009, 2013, 2014).

Elevated plasma levels of APR proteins are a recognized risk factor for CVD (Estabragh and Mamas, 2013; Johnson et al., 2004; Kaptoge et al., 2012; Libby et al., 2010; Lowe, 2001; Mezaki et al., 2003; Pai et al., 2004; Pussinen et al., 2007; Ridker et al., 2000; Rivera et al., 2013; Saber et al., 2013; Taubes, 2002). Epidemiological studies have established associations between particulate air pollution exposures and blood levels of CRP (Elliott et al., 2009; Barregard et al., 2006; Allen et al., 2011; Hertel et al., 2010; Ohlson et al., 2010). Increased blood levels of SAA and CRP were associated with future risk of CVD in the Nurses' Health Study (Ridker et al., 2000). The Nurses' Study reported that a 5-fold increase in blood SAA levels was associated with a 3-fold increased risk of coronary heart disease. Comparable increases in SAA3 levels were reported in the present study (7-fold increase, 28 days following pulmonary CNT_{Small} exposure) and in male mice by (Kim et al., 2014) (4-fold increase, one year following pulmonary MWCNT exposure), indicating that human exposure to doses comparable to those in

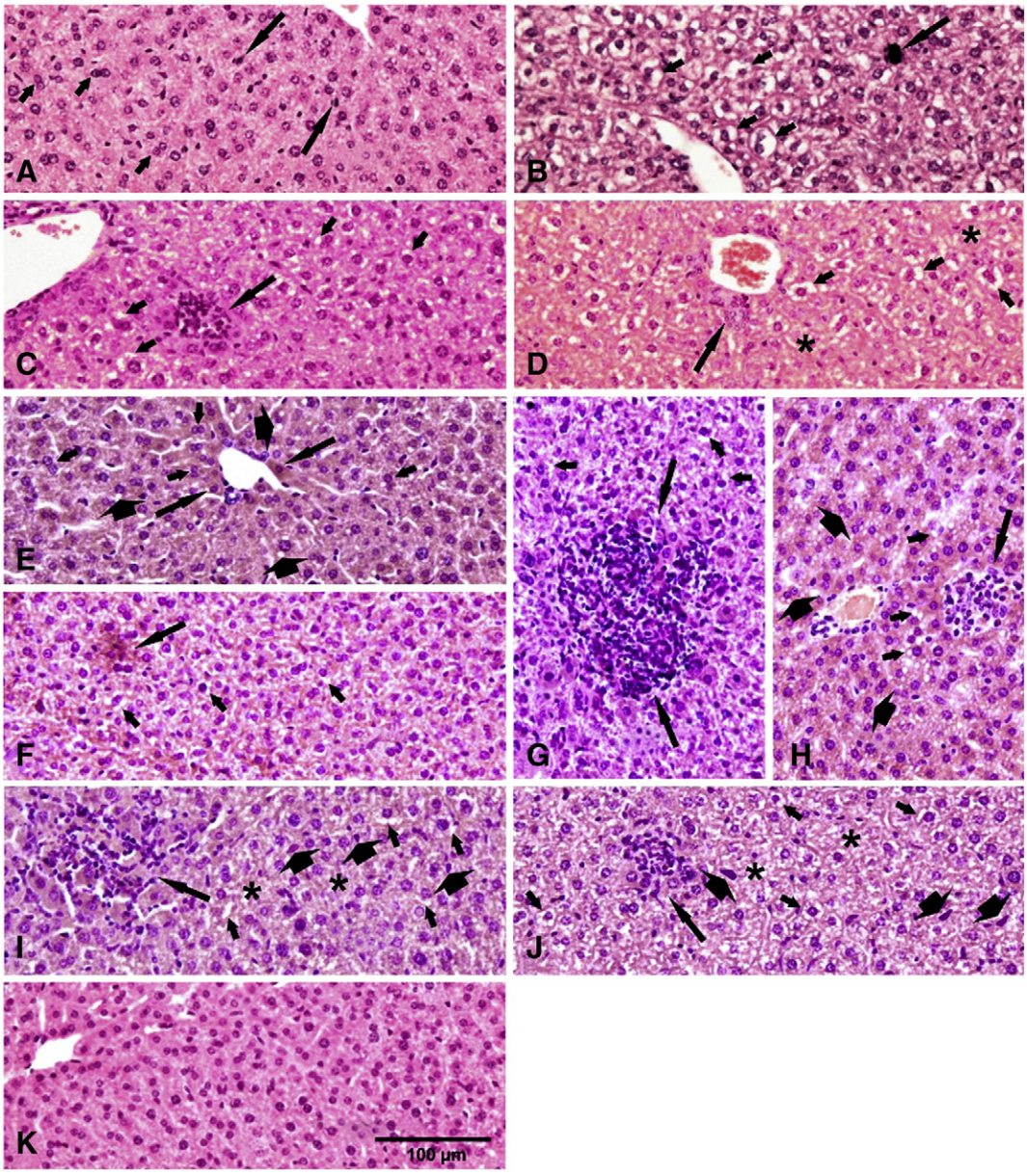

Fig. 4. Histopathologic findings in the liver. (A) 1 day after instillation (a.i.) of 54 µg CNT_{Small}: Hypertrophy of Kupffer cells (long arrows), numerous binucleate hepatocytes (short arrows). (B) 1 day a.i. of 162 µg CNT_{Small}: Macrophage (long arrow), central zonal vacuolar (hydropic) degeneration (short arrows). (C) 3 days a.i of 54 µg CNT_{Small}: Granuloma surrounded by eosinophilic necrotic hepatocytes (long arrow), vacuolar degeneration (short arrows); (D) 28 days a.i. of 162 µg CNT_{Small}: Foci of necrosis (asterisks), vacuolar degeneration (short arrows), hyperplasia of the bile ducts epithelium (long arrow). (E) 1 day a.i. of 162 µg CNT_{Large}: Eosinophilic necrotic hepatocytes surrounding central vein (long arrows), vacuolar degeneration of hepatocytes on the whole area of the liver lobule (head of arrows), and numerous binucleate hepatocytes (short arrows). (F) 3 days a.i. of 18 µg CNT_{Large}: Focus of eosinophilic necrotic hepatocytes (long arrow), vacuolar degeneration of hepatocytes on the whole area of the liver lobule (short arrows). (G) 3 days a.i. of 54 µg CNT_{Large}: Granuloma surrounded by eosinophilic necrotic hepatocytes (arrows), vacuolar degeneration (short arrows). (H) 3 days a.i. of 162 µg CNT_{Large}: Granuloma surrounded by eosinophilic necrotic hepatocytes (long arrow), vacuolar degeneration (short arrows), numerous binucleate hepatocytes (head of arrows). (I) 28 days a.i. of 54 µg CNT_{Large}: Granuloma surrounded by eosinophilic necrotic hepatocytes (long arrow), foci of necrosis (asterisks), vacuolar degeneration (short arrows), hypertrophy of Kupffer cells (head of arrows). (J) 28 days a.i. of 162 µg CNT_{Large}: Granuloma surrounded by eosinophilic necrotic hepatocytes (long arrow), foci of necrosis (asterisks), vacuolar degeneration (short arrows), hypertrophy of Kupffer cells (head of arrows). (K) typical microscopic pattern of the mouse liver — the control group. Staining HE, magnification on the figures A–J as scale in K.

these two murine studies may increase the risk of CVD in humans. Occupational studies have reported human CNT exposure levels of 10–300 µg/m^3 (Birch et al., 2011; Dahm et al., 2013; Erdely et al., 2013; Han et al., 2008; Lee et al., 2010; Maynard et al., 2004; Methner et al., 2010a, 2012). The highest dose in the present study corresponds to pulmonary deposition during a 40 year working life at 10 µg/m^3, or to pulmonary deposition during 1.5 work years at 300 µg/m^3. Furthermore, based on the observed strong correlation between plasma SAA3 levels and pulmonary *Saa3* mRNA levels, and the reported correlation between pulmonary neutrophil influx and pulmonary *Saa3* mRNA levels (Saber et al., 2013), pulmonary *Saa3* expression or neutrophil influx may be used as sensitive biomarkers of nanomaterial-induced acute phase response and may be used to group and rank nanomaterials in relation to possible CVD inducing potential.

The APR, and SAA in particular, affect blood lipid homeostasis and regulation of cholesterol biosynthesis (Bourdon et al., 2012a; Lindhorst et al., 1997; Saber et al., 2013, 2014). We show that pulmonary exposure to two very different MWCNTs induces changes in blood lipid composition that are similar to changes observed after systemically induced APR (Lindhorst et al., 1997). The data indicate that both MWCNTs cause perturbations in lipid-related processes as early as 1 day post-exposure, reaching their peak increases on day 3 and

completely reversed to basal levels by day 28 post-exposure. Thus, blood levels of HDL and LDL/VLDL cholesterol followed a time-course similar to what has been described for a strong APR in mice subcutaneously injected with silver nitrate (Lindhorst et al., 1997). During APR, SAA becomes incorporated into HDL thereby replacing ApoA-1 (Feingold and Grunfeld, 2010). Acute phase HDL is defective in reverse cholesterol transport, resulting in reduced cholesterol efflux from macrophages and lowered hepatic cholesterol excretion (Lindhorst et al., 1997; Banka et al., 1995; Artl et al., 2000; Annema et al., 2010).

We found that pulmonary exposures to the two very different MWCNTs elicit similar hepatic gene expression patterns. Whereas *Saa3* primarily drives the pulmonary APR (Bourdon et al., 2012a; Halappanavar et al., 2011; Saber et al., 2013, 2014), both *Saa1* and *Saa2* were differentially expressed as part of the hepatic APR. This is in agreement with previous observations (Uhlar and Whitehead, 1999). Functional analyses revealed that GO biological processes and IPA functions involved in cholesterol homeostasis and lipid metabolism were perturbed following exposure to both types of MWCNTs. This was driven, in part, by a uniform down-regulation of genes across the entire HMG-CoA reductase pathway (*Hmgcr*, *Mvk*, *Pmvk*, *Mvd*, *Fdps*, *Sqs*, *Sqle*, *Dhcr7*). Interestingly the opposite was observed in the lungs. In lungs, CNT_{Small} and CNT_{Large} induced consistent up-regulation of several genes involved in the HMG-CoA reductase pathway. The HMG-CoA reductase pathway is activated during low-sterol conditions and plays a central role both in the synthesis of cholesterol and in the production of intermediates for terpenoid synthesis, actin cytoskeleton remodeling, hormones and protein prenylation (Liao, 2002). However, the down-regulated expression levels of *Sqle* and *Dhcr7* in the liver indicate that MWCNT specifically targets cholesterol synthesis. The HMG-CoA reductase pathway is regulated by a negative feedback loop; the down-regulation is most likely due to the increased cholesterol levels in plasma (CNT_{Small} and CNT_{Large}) and liver (CNT_{Large} only).

In the present study, the systemic effects of MWCNT exposure were evaluated in female mice. Similarly increased plasma levels of SAA were recently reported for male mice exposed to MWCNTs (Kim et al., 2014). Lipoprotein profiles among pre-menopausal women differ from men's, as they have lower LDL cholesterol levels while HDL cholesterol levels are higher. Also, LDL cholesterol levels in post-menopausal women are equal to, or higher than, those in age-matched males, and can be lowered by hormone replacement therapy (Skafar et al., 1997). Thus, a cardioprotective effect of female sex hormones, particularly estrogen, has been proposed (Skafar et al., 1997; De Marinis et al., 2008). It is therefore possible that the differences in systemic HDL levels following MWCNT exposure observed between the study of (Kim et al., 2014) and our study are related to the gender of the experimental animals. A study in rats reported gender-related differences in the HMG-CoA reductase pathway, with females having lower activity and expression of 3-hydroxy 3-methylglutaryl coenzyme A reductase (*Hmgcr*), the rate-limiting enzyme in the HMG-CoA reductase pathway, compared to age-matched males (De Marinis et al., 2008). Similar differences were observed when comparing non-treated males with males treated with 17-β-estradiol, indicating an estrogen-reduction of the HMG-CoA reductase pathway. Thus, the present study adds to the overall weight of evidence of systemic acute phase response in mice following MWCNT exposure in both genders.

Studies in rodents have shown that severe inflammation, initiated through intraperitoneal injection of LPS, induces the hepatic HMG-CoA reductase pathway (Feingold et al., 1993, 1995; Memon et al., 1993). Perturbations in the hepatic HMG-CoA reductase pathways were also observed following pulmonary exposure to nano-CB (Bourdon et al., 2012a). However, the directions of the observed effects were opposite. HMG-CoA was up-regulated following nano-CB exposure, whereas, it was down-regulated following exposures to both types of MWCNTs. Another difference includes the down-regulation of *Ldlr* in the livers of MWCNTs exposed mice in the present study, but no effects following LPS and nano-CB exposure (Bourdon et al., 2012a; Feingold et al., 1993, 1995). *Ldlr* and *Hmgcr* are regulated in a coordinated fashion with parallel increases or decreases in mRNA levels in response to stimuli (Goldstein and Brown, 1990), as observed in the present study. *Ldlr* primarily facilitates the transport of VLDL, intermediate-density lipoproteins and LDL across the membrane (Lagor and Millar, 2010), and the hepatic down-regulation of *Ldlr* could in part explain the increased plasma levels of LDL/VLDL. Thus, the observed dissimilarities between our results and those of others (Bourdon et al., 2012a; Feingold et al., 1993, 1995) indicate that MWCNT exposure may elicit hepatic and systemic responses related to their structures, that differ from responses seen following LPS and nano-CB exposure.

The dissimilarities observed between nano-CB relative to MWCNT exposures may result from greater and more prolonged APR (observed at both mRNA and protein levels) following MWCNT exposure than those observed following nano-CB. Plasma SAA levels were at least 30-fold increased following MWCNT exposure, whereas a maximum increase of 15.6% has previously been observed following a similar nano-CB exposure (Bourdon et al., 2012a). The greater and prolonged APR would lead to a higher proportion of circulating HDL-SAA. Besides having decreased cholesterol efflux ability, HDL-SAA is also able to transform peripheral macrophages into foam cells, and to promote plaque progression in $APOE^{-/-}$ mice (Artl et al., 2000; Lee et al., 2013). Thus, our results indicate that increased HDL-SAA levels may present a significant risk factor for CVD following MWCNT exposure.

Supplementary Fig. 4 depicts the observed pulmonary, systemic and hepatic changes following pulmonary MWCNT exposure. In particular, we note that down-regulation of hepatic expression of *Abcg5* and *Abcg8* occurs following exposure to both types of MWCNTs (Supplementary Table 1). *Abcg5* and *Abcg8* encode biliary transporters that facilitate cholesterol excretion into the bile (Yu et al., 2002). Biliary excretion is a major function in reverse cholesterol transport, and decreased expression of *Abcg5* and *Abcg8* has been linked to retention of cholesterol in the liver (McGillicuddy et al., 2009). Due to the perturbations observed for many steps in the reverse cholesterol transport, it is possible that the observed increased APR may have a direct or indirect effect on bile excretion of cholesterol, which, in part, could explain the observed increase in hepatic cholesterol levels. In addition, our toxicogenomics analysis of hepatic gene expression revealed a general inflammatory response in the liver, which is known to affect bile excretion (McGillicuddy et al., 2009).

Intratracheal instillation of either type of MWCNTs in mice caused histological changes in the liver. An increased number of binucleate hepatocytes in MWCNT treated mice were observed, indicating hepatocytic regeneration typically seen after a toxic insult (Kostka et al., 2000). Similar increases in binucleated hepatocytes have previously been reported following nanoparticle-exposure (Hougaard et al., 2013; Kostka et al., 2000; Saber et al., 2012). Other indications of systemic MWCNT-induced mild liver injury in our study include the following: microfoci of necrosis, eosinophilic necrosis of single hepatocytes, and hepatocytes with pyknotic nuclei (Fig. 4 and Supplementary Table 5), which all are frequent sequels to liver injury (Haschek et al., 2010). MWCNT also induces hepatic inflammatory changes. Small foci of inflammatory cells, polymorphonuclear cell foci, macrophages, and granulomas were observed. Although scattered inflammatory cell accumulations are commonly observed in untreated mice (Haschek et al., 2010), these were more frequent in the MWCNT-treated mice. Increased numbers and/or hypertrophy of Kupffer cells could be related to one of their functions in the liver, production of mediators of inflammation (Harrada et al., 1999). Hepatic focal necrosis, single cell necrosis, inflammatory changes and hyperplasia or hypertrophy of Kupffer cells have been observed in mice after intratracheal instillation of other nanoparticles (Hougaard et al., 2013; Saber et al., 2012) and in rats exposed by inhalation to nanoparticles (Sung et al., 2009; Ji et al., 2007). The histological hepatic effects of exposure to the two MWCNTs are similar in types of lesions induced, but CNT_{Large} exposure causes larger granulomas, and the incidence of vacuolar degeneration tended to be

higher. Vacuolar degeneration was distributed throughout the whole area of the hepatic lobule and its location did not change with time. Also the eosinofilic necrosis of hepatocytes of a single row of hepatocytes surrounding the central vein was characteristic for livers from the CNT_{Large} exposure groups. In general the histological changes were not indicative of strong toxicity.

Although the gene expression patters were highly similar after exposure to either CNT, our data also indicated subtle differences in gene expression and lipid concentrations following CNT_{Small} or CNT_{Large} exposure. Only CNT_{Small} exposure resulted in changes in hepatic gene expression at day 28 and the number of differentially expressed genes was greater than that in the CNT_{Large} groups. CNT_{Small} caused an earlier onset in the down-regulation of the HMG-CoA reductase pathway than CNT_{Large}; the expression of *Ldlr* was differentially down-regulated even at the lowest dose at days 1 and 3 following CNT_{Small} exposure (Table 2). Exposure to CNT_{Large}, on the other hand, seemed to induce a greater hepatic APR in accordance with the recorded morphological inflammatory changes. However, despite these functional differences and different physicochemical properties, the responses following CNT_{Small} and CNT_{Large} exposures were more similar than different.

MWCNTs are HARN (high aspect ratio nanoparticles) and have, as such, been extensively discussed in relation to asbestos toxicity. Our results show that pulmonary exposure to MWCNT induces a pulmonary-based systemic APR resulting in changes in cholesterol homeostasis and liver morphology. We observed a close correlation between plasma SAA3 levels and pulmonary *Saa3* mRNA levels. We have previously demonstrated a close correlation between pulmonary *Saa3* levels and neutrophil influx (Saber et al., 2013, 2014; Halappanavar et al., 2014; Poulsen et al., 2014). The observed APR and increased cholesterol levels link MWCNT exposure to risk of CVD. Since Teeguarden et al. (2011) identified the same APR proteins in the lungs of mice following exposure to single-walled carbon nanotubes or asbestos, this suggests that asbestos exposure is likely to induce a similar pulmonary APR. In concordance with this, prospective studies on smoking-adjusted, occupational asbestos exposure have reported an association between exposure to asbestos and increased risk of ischaemic heart disease (Harding et al., 2012; Sanden et al., 1993). Thus, our findings in parallel with others suggest that MWCNT exposure increases the risk of CVD. The present work has established a correlation between pulmonary and systemic APR following pulmonary exposure to MWCNTs, and suggests that pulmonary APR can be used to group and rank different nanomaterials in relation to CVD inducing potential.

Conclusion

We show that pulmonary exposure to two very different MWCNTs induced very similar systemic APR, with induced alterations in plasma levels of APR proteins, cholesterol, LDL/VLDL and HDL, and changes in hepatic gene expression and liver morphology. Furthermore, we found a close correlation between plasma SAA3 levels and pulmonary *Saa3* mRNA levels. Taken together, the results link pulmonary exposure to MWCNTs with risk of CVD.

Supplementary data to this article can be found online at http://dx.doi.org/10.1016/j.taap.2015.01.011.

Conflict of interests

The authors declare that they have no competing interests.

Funding

The project was supported by grants from the National Research Centre for the Working Environment in Denmark and the Danish NanoSafety Center, grant# 20110092173-3, the European Community's Seventh Framework Programme (FP7/2007–2013) under grant agreement # 247989 (Nanosustain), and Health Canada's Chemical Management Plan-2 Nano research funds and Genomics Research and Development Initiative. The funders had no role in study design, data collection and analysis, decision to publish, or preparation of the manuscript.

Acknowledgments

The authors thank Michael Guldbrandsen, Lisbeth M Petersen, Marianne Lauridsen, Lourdes Petersen and Elzbieta Christiansen for their technical assistance.

References

Aiso, S., Kubota, H., Umeda, Y., Kasai, T., Takaya, M., Yamazaki, K., Nagano, K., Sakai, T., Koda, S., Fukushima, S., 2011. Translocation of intratracheally instilled multiwall carbon nanotubes to lung-associated lymph nodes in rats. Ind. Health 49, 215–220.

Allen, R.W., Carlsten, C., Karlen, B., Leckie, S., van, E.S., Vedal, S., Wong, I., Brauer, M., 2011. An air filter intervention study of endothelial function among healthy adults in a woodsmoke-impacted community. Am. J. Respir. Crit. Care Med. 183, 1222–1230.

Annema, W., Nijstad, N., Tolle, M., de Boer, J.F., Buijs, R.V., Heeringa, P., van der, G.M., and Tietge, U.J., 2010. Myeloperoxidase and serum amyloid A contribute to impaired in vivo reverse cholesterol transport during the acute phase response but not group IIA secretory phospholipase A(2). J. Lipid Res. 51, 743–754.

Artl, A., Marsche, G., Lestavel, S., Sattler, W., Malle, E., 2000. Role of serum amyloid A during metabolism of acute-phase HDL by macrophages. Arterioscler. Thromb. Vasc. Biol. 20, 763–772.

Banka, C.L., Yuan, T., de Beer, M.C., Kindy, M., Curtiss, L.K., de Beer, F.C., 1995. Serum amyloid A (SAA): influence on HDL-mediated cellular cholesterol efflux. J. Lipid Res. 36, 1058–1065.

Barregard, L., Sallsten, G., Gustafson, P., Andersson, L., Johansson, L., Basu, S., Stigendal, L., 2006. Experimental exposure to wood-smoke particles in healthy humans: effects on markers of inflammation, coagulation, and lipid peroxidation. Inhal. Toxicol. 18, 845–853.

Birch, M.E., Ku, B.K., Evans, D.E., Ruda-Eberenz, T.A., 2011. Exposure and emissions monitoring during carbon nanofiber production—Part I: elemental carbon and iron-soot aerosols. Ann. Occup. Hyg. 55, 1016–1036.

Bourdon, J.A., Halappanavar, S., Saber, A.T., Jacobsen, N.R., Williams, A., Wallin, H., Vogel, U., Yauk, C.L., 2012a. Hepatic and pulmonary toxicogenomic profiles in mice intratracheally instilled with carbon black nanoparticles reveal pulmonary inflammation, acute phase response, and alterations in lipid homeostasis. Toxicol. Sci. 127, 474–484.

Bourdon, J.A., Saber, A.T., Halappanavar, S., Jackson, P.A., Wu, D., Hougaard, K.S., Jacobsen, N.R., Williams, A., Vogel, U., Wallin, H., Yauk, C.L., 2012b. Carbon black nanoparticle intratracheal installation results in large and sustained changes in the expression of miR-135b in mouse lung. Environ. Mol. Mutagen. 53, 462–468.

Chen, L.C., Nadziejko, C., 2005. Effects of subchronic exposures to concentrated ambient particles (CAPs) in mice. V. CAPs exacerbate aortic plaque development in hyperlipidemic mice. Inhal. Toxicol. 17, 217–224.

Clancy, L., Goodman, P., Sinclair, H., Dockery, D.W., 2002. Effect of air-pollution control on death rates in Dublin, Ireland: an intervention study. Lancet 360, 1210–1214.

Czarny, B., Georgin, D., Berthon, F., Plastow, G., Pinault, M., Patriarche, G., Thuleau, A., L'Hermite, M.M., Taran, F., Dive, V., 2014. Carbon nanotube translocation to distant organs after pulmonary exposure: insights from in situ (14)c-radiolabeling and tissue radioimaging. ACS Nano 8, 5715–5724.

Dahm, M.M., Evans, D.E., Schubauer-Berigan, M.K., Birch, M.E., Deddens, J.A., 2013. Occupational exposure assessment in carbon nanotube and nanofiber primary and secondary manufacturers: mobile direct-reading sampling. Ann. Occup. Hyg. 57, 328–344.

De Marinis, E., Martini, C., Trentalance, A., Pallottini, V., 2008. Sex differences in hepatic regulation of cholesterol homeostasis. J. Endocrinol. 198, 635–643.

Dockery, D.W., Pope III, C.A., Xu, X., Spengler, J.D., Ware, J.H., Fay, M.E., Ferris Jr., B.G., Speizer, F.E., 1993. An association between air pollution and mortality in six U.S. cities. N. Engl. J. Med. 329, 1753–1759.

Dong, Z., Wu, T., Qin, W., An, C., Wang, Z., Zhang, M., Zhang, Y., Zhang, C., An, F., 2011. Serum amyloid A directly accelerates the progression of atherosclerosis in apolipoprotein E-deficient mice. Mol. Med. 17, 1357–1364.

Edgar, R., Barrett, T., 2006. NCBI GEO standards and services for microarray data. Nat. Biotechnol. 24, 1471–1472.

Elliott, P., Chambers, J.C., Zhang, W., Clarke, R., Hopewell, J.C., Peden, J.F., Erdmann, J., Braund, P., Engert, J.C., Bennett, D., Coin, L., Ashby, D., Tzoulaki, I., Brown, I.J., Mt-Isa, S., McCarthy, M.I., Peltonen, L., Freimer, N.B., Farrall, M., Ruokonen, A., Hamsten, A., Lim, N., Froguel, P., Waterworth, D.M., Vollenweider, P., Waeber, G., Jarvelin, M.R., Mooser, V., Scott, J., Hall, A.S., Schunkert, H., Anand, S.S., Collins, R., Samani, N.J., Watkins, H., Kooner, J.S., 2009. Genetic loci associated with C-reactive protein levels and risk of coronary heart disease. JAMA 302, 37–48.

Erdely, A., Hulderman, T., Salmen-Muniz, R., Liston, A., Zeidler-Erdely, P.C., Chen, B.T., Stone, S., Frazer, D.G., Antonini, J.M., Simeonova, P.P., 2011a. Inhalation exposure of gas–metal arc stainless steel welding fume increased atherosclerotic lesions in apolipoprotein E knockout mice. Toxicol. Lett. 204, 12–16.

Erdely, A., Liston, A., Salmen-Muniz, R., Hulderman, T., Young, S.H., Zeidler-Erdely, P.C., Castranova, V., Simeonova, P.P., 2011b. Identification of systemic markers from a pulmonary carbon nanotube exposure. J. Occup. Environ. Med. 53, S80–S86.

Erdely, A., Dahm, M., Chen, B.T., Zeidler-Erdely, P.C., Fernback, J.E., Birch, M.E., Evans, D.E., Kashon, M.L., Deddens, J.A., Hulderman, T., Bilgesu, S.A., Battelli, L., Schwegler-Berry, D., Leonard, H.D., McKinney, W., Frazer, D.G., Antonini, J.M., Porter, D.W., Castranova, V., Schubauer-Berigan, M.K., 2013. Carbon nanotube dosimetry: from workplace exposure assessment to inhalation toxicology. Part. Fibre Toxicol. 10, 53.

Estabragh, Z.R., Mamas, M.A., 2013. The cardiovascular manifestations of influenza: a systematic review. Int. J. Cardiol. 167, 2397–2403.

Feingold, K.R., Grunfeld, C., 2010. The acute phase response inhibits reverse cholesterol transport. J. Lipid Res. 51, 682–684.

Feingold, K.R., Hardardottir, I., Memon, R., Krul, E.J., Moser, A.H., Taylor, J.M., Grunfeld, C., 1993. Effect of endotoxin on cholesterol biosynthesis and distribution in serum lipoproteins in Syrian hamsters. J. Lipid Res. 34, 2147–2158.

Feingold, K.R., Pollock, A.S., Moser, A.H., Shigenaga, J.K., Grunfeld, C., 1995. Discordant regulation of proteins of cholesterol metabolism during the acute phase response. J. Lipid Res. 36, 1474–1482.

Folch, J., Lees, M., Sloane Stanley, G.H., 1957. A simple method for the isolation and purification of total lipides from animal tissues. J. Biol. Chem. 226, 497–509.

Gabay, C., Kushner, I., 1999. Acute-phase proteins and other systemic responses to inflammation. N. Engl. J. Med. 340, 448–454.

Goldstein, J.L., Brown, M.S., 1990. Regulation of the mevalonate pathway. Nature 343, 425–430.

Grosse, Y., Loomis, D., Guyton, K.Z., Lauby-Secretan, B., Ghissassi, F.E., Bouvard, V., Benbrahim-Tallaa, L., Guha, N., Scoccianti, C., Mattock, H., Straif, K., 2014. Carcinogenicity of fluoro-edenite, silicon carbide fibres and whiskers, and carbon nanotubes. Lancet Oncol. 15, 1427–1428.

Halappanavar, S., Jackson, P., Williams, A., Jensen, K.A., Hougaard, K.S., Vogel, U., Yauk, C.L., Wallin, H., 2011. Pulmonary response to surface-coated nanotitanium dioxide particles includes induction of acute phase response genes, inflammatory cascades, and changes in microRNAs: a toxicogenomic study. Environ. Mol. Mutagen. 52, 425–439.

Halappanavar, S., Saber, A.T., Decan, N., Jensen, K.A., Wu, D., Jacobsen, N.R., Guo, C., Rogowski, J., Koponen, I.K., Levin, M., Madsen, A.M., Atluri, R., Snitka, V., Birkedal, R.K., Rickerby, D., Williams, A., Wallin, H., Yauk, C., Vogel, U., 2014. Transcriptional profiling identifies physicochemical properties of nanomaterials that are determinants of the in vivo pulmonary response. Environ. Mol. Mutagen. http://dx.doi.org/10.1002/em.21936 ([Epub ahead of print]).

Han, J.H., Lee, E.J., Lee, J.H., So, K.P., Lee, Y.H., Bae, G.N., Lee, S.B., Ji, J.H., Cho, M.H., Yu, I.J., 2008. Monitoring multiwalled carbon nanotube exposure in carbon nanotube research facility. Inhal. Toxicol. 20, 741–749.

Harding, A.H., Darnton, A., Osman, J., 2012. Cardiovascular disease mortality among British asbestos workers (1971–2005). Occup. Environ. Med. 69, 417–421.

Harrada, T., Enomoto, A., Boorman, G.A., Maronpot, R.R., 1999. Chapter 7: liver and gallbladder. In: Maronpot, R.R., Boorman, G.A., Gaul, B.W. (Eds.), Pathology of the Mouse. Cache River Press, pp. 119–171.

Haschek, W.M., Rousseaux, C.G., Wallig, M.A., 2010. Fundamentals of Toxicologic Pathology, Chapter 9: The Liver. Academic Press.

Hertel, S., Viehmann, A., Moebus, S., Mann, K., Brocker-Preuss, M., Mohlenkamp, S., Nonnemacher, M., Erbel, R., Jakobs, H., Memmesheimer, M., Jockel, K.H., Hoffmann, B., 2010. Influence of short-term exposure to ultrafine and fine particles on systemic inflammation. Eur. J. Epidemiol. 25, 581–592.

Hoffman, J.S., Benditt, E.P., 1983. Plasma clearance kinetics of the amyloid-related high density lipoprotein apoprotein, serum amyloid protein (apoSAA), in the mouse. Evidence for rapid apoSAA clearance. J. Clin. Invest. 71, 926–934.

Hougaard, K.S., Jackson, P., Kyjovska, Z.O., Birkedal, R.K., De Temmerman, P.J., Brunelli, A., Verleysen, E., Madsen, A.M., Saber, A.T., Pojana, G., Mast, J., Marcomini, A., Jensen, K.A., Wallin, H., Szarek, J., Mortensen, A., Vogel, U., 2013. Effects of lung exposure to carbon nanotubes on female fertility and pregnancy. A study in mice. Reprod. Toxicol. 41, 86–97.

Huang, D.W., Sherman, B.T., Lempicki, R.A., 2009a. Systematic and integrative analysis of large gene lists using DAVID. Nucleic Acids Res. 37 (1), 1–13.

Huang, D.W., Sherman, B.T., Lempicki, R.A., 2009b. Systematic and integrative analysis of large gene lists using DAVID bioinformatics resources. Nat. Protoc. 4, 44–57.

Husain, M., Saber, A.T., Guo, C., Jacobsen, N.R., Jensen, K.A., Yauk, C.L., Williams, A., Vogel, U., Wallin, H., Halappanavar, S., 2013. Pulmonary instillation of low doses of titanium dioxide nanoparticles in mice leads to particle retention and gene expression changes in the absence of inflammation. Toxicol. Appl. Pharmacol. 269, 250–262.

Jackson, P., Hougaard, K.S., Boisen, A.M., Jacobsen, N.R., Jensen, K.A., Moller, P., Brunborg, G., Gutzkow, K.B., Andersen, O., Loft, S., Vogel, U., Wallin, H., 2011. Pulmonary exposure to carbon black by inhalation or instillation in pregnant mice: effects on liver DNA strand breaks in dams and offspring. Nanotoxicology 6, 486–500.

Jackson, P., Kling, K., Jensen, K.A., Clausen, P.A., Madsen, A.M., Wallin, H., Vogel, U., 2014. Characterization of genotoxic response to 15 multiwalled carbon nanotubes with variable physicochemical properties including surface functionalizations in the FE1-Muta (TM) mouse lung epithelial cell line. Environ. Mol. Mutagen. http://dx.doi.org/10.1002/em.21922 ([Epub ahead of print]).

Ji, J.H., Jung, J.H., Kim, S.S., Yoon, J.U., Park, J.D., Choi, B.S., Chung, Y.H., Kwon, I.H., Jeong, J., Han, B.S., Shin, J.H., Sung, J.H., Song, K.S., Yu, I.J., 2007. Twenty-eight-day inhalation toxicity study of silver nanoparticles in Sprague–Dawley rats. Inhal. Toxicol. 19, 857–871.

Johnson, B.D., Kip, K.E., Marroquin, O.C., Ridker, P.M., Kelsey, S.F., Shaw, L.J., Pepine, C.J., Sharaf, B., Bairey Merz, C.N., Sopko, G., Olson, M.B., Reis, S.E., 2004. Serum amyloid A as a predictor of coronary artery disease and cardiovascular outcome in women: the National Heart, Lung, and Blood Institute-Sponsored Women's Ischemia Syndrome Evaluation (WISE). Circulation 109, 726–732.

Kaptoge, S., Di, A.E., Pennells, L., Wood, A.M., White, I.R., Gao, P., Walker, M., Thompson, A., Sarwar, N., Caslake, M., Butterworth, A.S., Amouyel, P., Assmann, G., Bakker, S.J., Barr, E.L., Barrett-Connor, E., Benjamin, E.J., Bjorkelund, C., Brenner, H., Brunner, E., Clarke, R., Cooper, J.A., Cremer, P., Cushman, M., Dagenais, G.R., D'Agostino Sr., R.B., Dankner, R., vey-Smith, G., Deeg, D., Dekker, J.M., Engstrom, G., Folsom, A.R., Fowkes, F.G., Gallacher, J., Gaziano, J.M., Giampaoli, S., Gillum, R.F., Hofman, A., Howard, B.V., Ingelsson, E., Iso, H., Jorgensen, T., Kiechl, S., Kitamura, A., Kiyohara, Y., Koenig, W., Kromhout, D., Kuller, L.H., Lawlor, D.A., Meade, T.W., Nissinen, A., Nordestgaard, B.G., Onat, A., Panagiotakos, D.B., Psaty, B.M., Rodriguez, B., Rosengren, A., Salomaa, V., Kauhanen, J., Salonen, J.T., Shaffer, J.A., Shea, S., Ford, I., Stehouwer, C.D., Strandberg, T.E., Tipping, R.W., Tosetto, A., Wassertheil-Smoller, S., Wennberg, P., Westendorp, R.G., Whincup, P.H., Wilhelmsen, L., Woodward, M., Lowe, G.D., Wareham, N.J., Khaw, K.T., Sattar, N., Packard, C.J., Gudnason, V., Ridker, P.M., Pepys, M.B., Thompson, S.G., Danesh, J., 2012. C-Reactive protein, fibrinogen, and cardiovascular disease prediction. N. Engl. J. Med. 367, 1310–1320.

Kim, J.E., Lee, S., Lee, A.Y., Seo, H.W., Chae, C., Cho, M.H., 2014. Intratracheal exposure to multi-walled carbon nanotubes induces a nonalcoholic steatohepatitis-like phenotype in C57BL/6J mice. Nanotoxicology 1–11 [Epub ahead of print].

Kobler, C., Saber, A.T., Jacobsen, N.R., Wallin, H., Vogel, U., Qvortrup, K., Molhave, K., 2014. FIB-SEM imaging of carbon nanotubes in mouse lung tissue. Anal. Bioanal. Chem. 406, 3863–3873.

Kobler, C., Poulsen, S.S., Saber, A.T., Jacobsen, N.R., Wallin, H., Yauk, C., Halappanavar, S., Vogel, U., Qvortrup, K., Molhave, K., 2015. Time-dependent subcellular distribution and effects of carbon nanotubes in lungs of mice. PLoS One 10 (1), e0116481.

Kostka, G., Palut, D., Kopec-Szlezak, J., Ludwicki, J.K., 2000. Early hepatic changes in rats induced by permethrin in comparison with DDT. Toxicology 142, 135–143.

Lagor, W.R., Millar, J.S., 2010. Overview of the LDL receptor: relevance to cholesterol metabolism and future approaches for the treatment of coronary heart disease. J. Recept. Ligand Channel Res. 3, 1–12.

Lee, J.H., Lee, S.B., Bae, G.N., Jeon, K.S., Yoon, J.U., Ji, J.H., Sung, J.H., Lee, B.G., Lee, J.H., Yang, J.S., Kim, H.Y., Kang, C.S., Yu, I.J., 2010. Exposure assessment of carbon nanotube manufacturing workplaces. Inhal. Toxicol. 22, 369–381.

Lee, H.Y., Kim, S.D., Baek, S.H., Choi, J.H., Cho, K.H., Zabel, B.A., Bae, Y.S., 2013. Serum amyloid A stimulates macrophage foam cell formation via lectin-like oxidized low-density lipoprotein receptor 1 upregulation. Biochem. Biophys. Res. Commun. 433, 18–23.

Li, Z., Hulderman, T., Salmen, R., Chapman, R., Leonard, S.S., Young, S.H., Shvedova, A., Luster, M.I., Simeonova, P.P., 2007. Cardiovascular effects of pulmonary exposure to single-wall carbon nanotubes. Environ. Health Perspect. 115, 377–382.

Liao, J.K., 2002. Isoprenoids as mediators of the biological effects of statins. J. Clin. Invest. 110, 285–288.

Libby, P., Okamoto, Y., Rocha, V.Z., Folco, E., 2010. Inflammation in atherosclerosis: transition from theory to practice. Circ. J. 74, 213–220.

Lindhorst, E., Young, D., Bagshaw, W., Hyland, M., Kisilevsky, R., 1997. Acute inflammation, acute phase serum amyloid A and cholesterol metabolism in the mouse. Biochim. Biophys. Acta 1339, 143–154.

Lowe, G.D., 2001. The relationship between infection, inflammation, and cardiovascular disease: an overview. Ann. Periodontol. 6, 1–8.

Ma-Hock, L., Treumann, S., Strauss, V., Brill, S., Luizi, F., Mertler, M., Wiench, K., Gamer, A.O., van Ravenzwaay, B., Landsiedel, R., 2009. Inhalation toxicity of multiwall carbon nanotubes in rats exposed for 3 months. Toxicol. Sci. 112, 468–481.

Maynard, A.D., Baron, P.A., Foley, M., Shvedova, A.A., Kisin, E.R., Castranova, V., 2004. Exposure to carbon nanotube material: aerosol release during the handling of unrefined single-walled carbon nanotube material. J. Toxicol. Environ. Health A 67, 87–107.

McGillicuddy, F.C., de la Llera, M.M., Hinkle, C.C., Joshi, M.R., Chiquoine, E.H., Billheimer, J.T., Rothblat, G.H., Reilly, M.P., 2009. Inflammation impairs reverse cholesterol transport in vivo. Circulation 119, 1135–1145.

Meek, R.L., Eriksen, N., Benditt, E.P., 1992. Murine serum amyloid A3 is a high density apolipoprotein and is secreted by macrophages. Proc. Natl. Acad. Sci. U. S. A. 89, 7949–7952.

Memon, R.A., Grunfeld, C., Moser, A.H., Feingold, K.R., 1993. Tumor necrosis factor mediates the effects of endotoxin on cholesterol and triglyceride metabolism in mice. Endocrinology 132, 2246–2253.

Mercer, R.R., Scabilloni, J.F., Hubbs, A.F., Wang, L., Battelli, L.A., McKinney, W., Castranova, V., Porter, D.W., 2013. Extrapulmonary transport of MWCNT following inhalation exposure. Part. Fibre Toxicol. 10, 38.

Methner, M., Hodson, L., Dames, A., Geraci, C., 2010a. Nanoparticle emission assessment technique (NEAT) for the identification and measurement of potential inhalation exposure to engineered nanomaterials—part B: results from 12 field studies. J. Occup. Environ. Hyg. 7, 163–176.

Methner, M., Hodson, L., Geraci, C., 2010b. Nanoparticle emission assessment technique (NEAT) for the identification and measurement of potential inhalation exposure to engineered nanomaterials—part A. J. Occup. Environ. Hyg. 7, 127–132.

Methner, M., Beaucham, C., Crawford, C., Hodson, L., Geraci, C., 2012. Field application of the nanoparticle emission assessment technique (NEAT): task-based air monitoring during the processing of engineered nanomaterials (ENM) at four facilities. J. Occup. Environ. Hyg. 9, 543–555.

Mezaki, T., Matsubara, T., Hori, T., Higuchi, K., Nakamura, A., Nakagawa, I., Imai, S., Ozaki, K., Tsuchida, K., Nasuno, A., Tanaka, T., Kubota, K., Nakano, M., Miida, T., Aizawa, Y., 2003. Plasma levels of soluble thrombomodulin, C-reactive protein, and serum amyloid A protein in the atherosclerotic coronary circulation. Jpn. Heart J. 44, 601–612.

Mikkelsen, L., Sheykhzade, M., Jensen, K.A., Saber, A.T., Jacobsen, N.R., Vogel, U., Wallin, H., Loft, S., Moller, P., 2011. Modest effect on plaque progression and vasodilatory function in atherosclerosis-prone mice exposed to nanosized TiO(2). Part. Fibre Toxicol. 8, 32.

NIOSH, 2013. Current Intelligence Bulletin 65: Occupational Exposure to Carbon Nanotubes and Nanofibers. Howard, J.

Ohlson, C.G., Berg, P., Bryngelsson, I.L., Elihn, K., Ngo, Y., Westberg, H., Sjogren, B., 2010. Inflammatory markers and exposure to occupational air pollutants. Inhal. Toxicol. 22, 1083–1090.

Pai, J.K., Pischon, T., Ma, J., Manson, J.E., Hankinson, S.E., Joshipura, K., Curhan, G.C., Rifai, N., Cannuscio, C.C., Stampfer, M.J., Rimm, E.B., 2004. Inflammatory markers and the risk of coronary heart disease in men and women. N. Engl. J. Med. 351, 2599–2610.

Park, E.J., Cho, W.S., Jeong, J., Yi, J., Choi, K., Park, K., 2009. Pro-inflammatory and potential allergic responses resulting from B cell activation in mice treated with multi-walled carbon nanotubes by intratracheal instillation. Toxicology 259, 113–121.

Pauluhn, J., 2010a. Multi-walled carbon nanotubes (Baytubes): approach for derivation of occupational exposure limit. Regul. Toxicol. Pharmacol. 57, 78–89.

Pauluhn, J., 2010b. Subchronic 13-week inhalation exposure of rats to multiwalled carbon nanotubes: toxic effects are determined by density of agglomerate structures, not fibrillar structures. Toxicol. Sci. 113, 226–242.

Pope III, C.A., Thun, M.J., Namboodiri, M.M., Dockery, D.W., Evans, J.S., Speizer, F.E., Heath Jr., C.W., 1995. Particulate air pollution as a predictor of mortality in a prospective study of U.S. adults. Am. J. Respir. Crit. Care Med. 151, 669–674.

Pope III, C.A., Burnett, R.T., Thurston, G.D., Thun, M.J., Calle, E.E., Krewski, D., Godleski, J.J., 2004. Cardiovascular mortality and long-term exposure to particulate air pollution: epidemiological evidence of general pathophysiological pathways of disease. Circulation 109, 71–77.

Porter, D.W., Hubbs, A.F., Mercer, R.R., Wu, N., Wolfarth, M.G., Sriram, K., Leonard, S., Battelli, L., Schwegler-Berry, D., Friend, S., Andrew, M., Chen, B.T., Tsuruoka, S., Endo, M., Castranova, V., 2010. Mouse pulmonary dose- and time course-responses induced by exposure to multi-walled carbon nanotubes. Toxicology 269, 136–147.

Porter, D.W., Hubbs, A.F., Chen, B.T., McKinney, W., Mercer, R.R., Wolfarth, M.G., Battelli, L., Wu, N., Sriram, K., Leonard, S., Andrew, M., Willard, P., Tsuruoka, S., Endo, M., Tsukada, T., Munekane, F., Frazer, D.G., Castranova, V., 2013. Acute pulmonary dose-responses to inhaled multi-walled carbon nanotubes. Nanotoxicology 7, 1179–1194.

Poulsen, S.S., Jacobsen, N.R., Labib, S., Wu, D., Husain, M., Williams, A., Bogelund, J.P., Andersen, O., Kobler, C., Molhave, K., Kyjovska, Z.O., Saber, A.T., Wallin, H., Yauk, C.L., Vogel, U., Halappanavar, S., 2013. Transcriptomic analysis reveals novel mechanistic insight into murine biological responses to multi-walled carbon nanotubes in lungs and cultured lung epithelial cells. PLoS One 8, e80452.

Poulsen, S.S., Saber, A.T., Williams, A., Andersen, O., Kobler, C., Atluri, R., Pozzebon, M.E., Mucelli, S.P., Simion, M., Rickerby, D., Mortensen, A., Jackson, P., Kyjovska, Z.O., Molhave, K., Jacobsen, N.R., Jensen, K.A., Yauk, C.L., Wallin, H., Halappanavar, S., Vogel, U., 2015. MWCNT of different physicochemical properties cause similar inflammatory responses, but differences in transcriptional and histological markers of fibrosis in mouse lungs. Toxicol. Appl. Pharmacol. 284, 16–32.

Pussinen, P.J., Tuomisto, K., Jousilahti, P., Havulinna, A.S., Sundvall, J., Salomaa, V., 2007. Endotoxemia, immune response to periodontal pathogens, and systemic inflammation associate with incident cardiovascular disease events. Arterioscler. Thromb. Vasc. Biol. 27, 1433–1439.

Reddy, A.R., Reddy, Y.N., Krishna, D.R., Himabindu, V., 2010. Pulmonary toxicity assessment of multiwalled carbon nanotubes in rats following intratracheal instillation. Environ. Toxicol. 27, 211–219.

Ridker, P.M., Hennekens, C.H., Buring, J.E., Rifai, N., 2000. C-Reactive protein and other markers of inflammation in the prediction of cardiovascular disease in women. N. Engl. J. Med. 342, 836–843.

Rivera, M.F., Lee, J.Y., Aneja, M., Goswami, V., Liu, L., Velsko, I.M., Chukkapalli, S.S., Bhattacharyya, I., Chen, H., Lucas, A.R., Kesavalu, L.N., 2013. Polymicrobial infection with major periodontal pathogens induced periodontal disease and aortic atherosclerosis in hyperlipidemic ApoE (null) mice. PLoS One 8, e57178.

Saber, A.T., Halappanavar, S., Folkmann, J.K., Bornholdt, J., Boisen, A.M., Moller, P., Williams, A., Yauk, C., Vogel, U., Loft, S., Wallin, H., 2009. Lack of acute phase response in the livers of mice exposed to diesel exhaust particles or carbon black by inhalation. Part. Fibre Toxicol. 6, 12.

Saber, A.T., Jacobsen, N.R., Mortensen, A., Szarek, J., Jackson, P., Madsen, A.M., Jensen, K.A., Koponen, I.K., Brunborg, G., Gutzkow, K.B., Vogel, U., Wallin, H., 2012. Nanotitanium dioxide toxicity in mouse lung is reduced in sanding dust from paint. Part. Fibre Toxicol. 9, 4.

Saber, A.T., Lamson, J.S., Jacobsen, N.R., Ravn-Haren, G., Hougaard, K.S., Nyendi, A.N., Wahlberg, P., Madsen, A.M., Jackson, P., Wallin, H., Vogel, U., 2013. Particle-induced pulmonary acute phase response correlates with neutrophil influx linking inhaled particles and cardiovascular risk. PLoS One 8, e69020.

Saber, A.T., Jacobsen, N.R., Jackson, P., Poulsen, S.S., Kyjovska, Z.O., Halappanavar, S., Yauk, C.L., Wallin, H., Vogel, U., 2014. Particle-induced pulmonary acute phase response may be the causal link between particle inhalation and cardiovascular disease. Wiley Interdiscip. Rev. Nanomed. Nanobiotechnol. 6, 517–531.

Salazar, A., Mana, J., Fiol, C., Hurtado, I., Argimon, J.M., Pujol, R., Pinto, X., 2000. Influence of serum amyloid A on the decrease of high density lipoprotein-cholesterol in active sarcoidosis. Atherosclerosis 152, 497–502.

Sanden, A., Jarvholm, B., Larsson, S., 1993. The importance of lung function, non-malignant diseases associated with asbestos, and symptoms as predictors of ischaemic heart disease in shipyard workers exposed to asbestos. Br. J. Ind. Med. 50, 785–790.

Shvedova, A.A., Kisin, E., Murray, A.R., Johnson, V.J., Gorelik, O., Arepalli, S., Hubbs, A.F., Mercer, R.R., Keohavong, P., Sussman, N., Jin, J., Yin, J., Stone, S., Chen, B.T., Deye, G., Maynard, A., Castranova, V., Baron, P.A., Kagan, V.E., 2008. Inhalation vs. aspiration of single-walled carbon nanotubes in C57BL/6 mice: inflammation, fibrosis, oxidative stress, and mutagenesis. Am. J. Physiol. Lung Cell. Mol. Physiol. 295, L552–L565.

Skafar, D.F., Xu, R., Morales, J., Ram, J., Sowers, J.R., 1997. Clinical review 91: female sex hormones and cardiovascular disease in women. J. Clin. Endocrinol. Metab. 82, 3913–3918.

Snyder-Talkington, B.N., Dymacek, J., Porter, D.W., Wolfarth, M.G., Mercer, R.R., Pacurari, M., Denvir, J., Castranova, V., Qian, Y., Guo, N.L., 2013. System-based identification of toxicity pathways associated with multi-walled carbon nanotube-induced pathological responses. Toxicol. Appl. Pharmacol. 272, 476–489.

Stapleton, P.A., Minarchick, V.C., Cumpston, A.M., McKinney, W., Chen, B.T., Sager, T.M., Frazer, D.G., Mercer, R.R., Scabilloni, J., Andrew, M.E., Castranova, V., Nurkiewicz, T.R., 2012. Impairment of coronary arteriolar endothelium-dependent dilation after multi-walled carbon nanotube inhalation: a time-course study. Int. J. Mol. Sci. 13, 13781–13803.

Sung, J.H., Ji, J.H., Park, J.D., Yoon, J.U., Kim, D.S., Jeon, K.S., Song, M.Y., Jeong, J., Han, B.S., Han, J.H., Chung, Y.H., Chang, H.K., Lee, J.H., Cho, M.H., Kelman, B.J., Yu, I.J., 2009. Subchronic inhalation toxicity of silver nanoparticles. Toxicol. Sci. 108, 452–461.

Taubes, G., 2002. Cardiovascular disease. Does inflammation cut to the heart of the matter? Science 296, 242–245.

Teeguarden, J.G., Webb-Robertson, B.J., Waters, K.M., Murray, A.R., Kisin, E.R., Varnum, S.M., Jacobs, J.M., Pounds, J.G., Zanger, R.C., Shvedova, A.A., 2011. Comparative proteomics and pulmonary toxicity of instilled single-walled carbon nanotubes, crocidolite asbestos, and ultrafine carbon black in mice. Toxicol. Sci. 120, 123–135.

Uhlar, C.M., Whitehead, A.S., 1999. Serum amyloid A, the major vertebrate acute-phase reactant. Eur. J. Biochem. 265, 501–523.

Wang, X., Katwa, P., Podila, R., Chen, P., Ke, P.C., Rao, A.M., Walters, D.M., Wingard, C.J., Brown, J.M., 2011. Multi-walled carbon nanotube instillation impairs pulmonary function in C57BL/6 mice. Part. Fibre Toxicol. 8, 24.

World Health Organization, World Heart Federation, World Stroke Organization, 2011. In: Mendes, S., Puska, P., Norrving, B. (Eds.), Global Atlas on Cardiovascular Disease Prevention and Control. World Health Organization, Geneva, pp. 1–164.

Yu, L., Li-Hawkins, J., Hammer, R.E., Berge, K.E., Horton, J.D., Cohen, J.C., Hobbs, H.H., 2002. Overexpression of ABCG5 and ABCG8 promotes biliary cholesterol secretion and reduces fractional absorption of dietary cholesterol. J. Clin. Invest. 110, 671–680.